

AD-A126 068

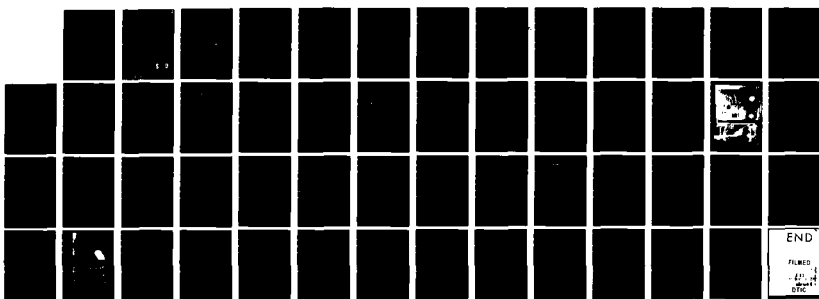
METAL COATED OPTICAL FIBERS FOR SENSORS(U) HONEYWELL  
CORPORATE TECHNOLOGY CENTER BLOOMINGTON MN  
G B HOCKER ET AL. MAR 83 N00173-88-C-0424

1/1

UNCLASSIFIED

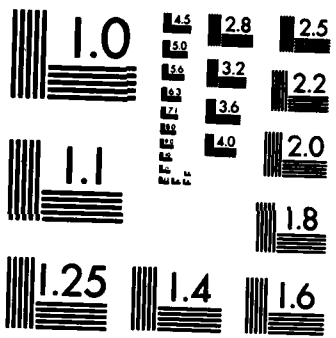
F/G 11/3

NL



END

FILMED  
- 11 -  
000



MICROCOPY RESOLUTION TEST CHART  
NATIONAL BUREAU OF STANDARDS-1963-A

DA 126068

(12)

METAL COATED OPTICAL FIBERS FOR SENSORS

CONTRACT N00173-80-C-0424

FINAL REPORT FOR PERIOD 08 SEPT. 1980 TO 31 DEC. 1982

MARCH 1983

BY

G. BENJAMIN HOCKER, JOHN SKOGEN  
HONEYWELL CORPORATE TECHNOLOGY CENTER  
10701 LYNDALE AVE. SO.  
BLOOMINGTON, MN 55420

FOR

NAVAL RESEARCH LABORATORY  
4555 OVERLOOK AVE. SW  
WASHINGTON, DC 20375

DTIC FILE COPY  
DTIC

This document has been approved  
for public release and does not  
contain recommendations or conclusions  
of the Defense Technical Information Center.  
DTIC

DTIC  
ELECTED  
MAR 25 1983  
S E D

129

TABLE OF CONTENTS

- I. INTRODUCTION
- II. THEORETICAL ANALYSIS
  - A. CALCULATIONS OF ACOUSTIC DESENSITIZATION OF TWO-LAYER METAL-COATED OPTICAL FIBER.
  - B. ANALYSIS OF MAGNETIC SENSITIVITY OF OPTICAL FIBER COATED WITH MAGNETOSTRICTIVE MATERIAL.
- III. UNDERCOATINGS
  - A. FREEZE COATING
  - B. SPUTTER DEPOSITION
  - C. ELECTROLESS NICKEL DEPOSITION
- IV. NICKEL ELECTROPLATING
  - A. PLATING BATHS
  - B. NICKEL ON PLANAR SUBSTRATES
  - C. NICKEL PLATING ON OPTICAL FIBERS
  - D. PLATING OF ALUMINUM-UNDERCOATED FIBERS
- V. ANNEALING
- VI. TEST PROCEDURES
  - A. B-H LOOPS
  - B. MAGNETOSTRICTION MEASUREMENTS
- VII. TEST RESULTS
  - A. B-H LOOP DATA
  - B. MAGNETOSTRICTION MEASUREMENTS ON PLANAR SUBSTRATES
  - C. FURTHER OBSERVATIONS
- VIII. FIBERS DELIVERED
- IX. CONCLUSIONS AND RECOMMENDATIONS
  - A. ACOUSTIC DESENSITIZED FIBERS
  - B. MAGNETICALLY SENSITIZED FIBERS
- X. REFERENCES

APPENDIX A: Published paper "Acoustic desensitization of single-mode fibers utilizing nickel coatings."

Accession For	
NTIS GRAF <input checked="" type="checkbox"/>	
DTIC TAB <input type="checkbox"/>	
Unannounced <input type="checkbox"/>	
Justification _____	
By _____	
Distribution/ _____	
Availability Codes	
Dist	Avail and/or Special
A	



**Unclassified**

SECURITY CLASSIFICATION OF THIS PAGE (When Data Entered)

<b>REPORT DOCUMENTATION PAGE</b>		<b>READ INSTRUCTIONS BEFORE COMPLETING FORM</b>
1. REPORT NUMBER	2. GOVT ACCESSION NO.	3. RECIPIENT'S CATALOG NUMBER
		AD-A126068
4. TITLE (and Subtitle) Metal Coated Optical Fibers For Sensors		5. TYPE OF REPORT & PERIOD COVERED Final Report 80 Sept. 08 to 82 Dec. 31
		6. PERFORMING ORG. REPORT NUMBER
7. AUTHOR(s) G. Benjamin Hocker and John D. Skogen		8. CONTRACT OR GRANT NUMBER(s) N00173-80-C-0424
9. PERFORMING ORGANIZATION NAME AND ADDRESS Honeywell Corporate Technology Center 10701 Lyndale Ave. So. Bloomington, MN 55420		10. PROGRAM ELEMENT, PROJECT, TASK AREA & WORK UNIT NUMBERS
11. CONTROLLING OFFICE NAME AND ADDRESS Naval Research Laboratory 4555 Overlook Ave. SW Washington, DC 20375		12. REPORT DATE January 1983
14. MONITORING AGENCY NAME & ADDRESS (if different from Controlling Office)		13. NUMBER OF PAGES
		15. SECURITY CLASS. (of this report) Unclassified
		15a. DECLASSIFICATION/DOWNGRADING SCHEDULE
16. DISTRIBUTION STATEMENT (of this Report)  Approved for public release Distribution unlimited		
17. DISTRIBUTION STATEMENT (of the abstract entered in Block 20, if different from Report)		
18. SUPPLEMENTARY NOTES		
19. KEY WORDS (Continue on reverse side if necessary and identify by block number) Fiber optics Sensors Acoustic Sensors Magnetic Sensors Coatings		
20. ABSTRACT (Continue on reverse side if necessary and identify by block number) This report describes techniques for applying nickel coatings to optical fibers by electroplating. The purpose is to produce optical fibers for sensors which are acoustically insensitive, and fibers which are magnetically sensitive.		

## METAL COATED OPTICAL FIBERS FOR SENSORS

### I. INTRODUCTION

Fiber optic interferometric sensors using single-mode fibers have attracted much attention as sensitive, geometrically-flexible acoustic sensors having flat, low-frequency response. An acoustic pressure strains the fiber, modulating the phase of the transmitted light, which is detected by the interferometer. The key to sensitivity control is in the elastic coatings applied to the fibers; the choice of coating material and thickness can serve to enhance or to reduce the acoustic sensitivity of the coated fiber.

In a similar fashion, the use of a magnetostrictive coating on an optical fiber allows its use in an interferometric sensor to measure magnetic fields. The sensitivity is provided by the strain induced by the coating material in a magnetic field.

The work carried out under this contract sought to enhance coating technology to provide metal coated optical fibers of benefit to both acoustic and magnetic versions of fiber optic interferometric sensors. Specifically, the objectives were (1) to demonstrate the feasibility of magnetostrictive coated optical fiber for sensing small magnetic fields, and (2) to demonstrate high-modulus coatings for acoustic desensitization of optical fibers. Although the two objectives are separate, predictions and subsequent results showed that nickel coatings applied to optical fibers can meet both requirements. This is because nickel is both a relatively good magnetostrictive material and has a high elastic modulus required for acoustic desensitization.

The method chosen to apply the nickel is electroplating, because it is relatively fast, low cost, and adaptable to a continuous coating line operation. The latter feature is necessary to apply coatings to the long fiber lengths required by most fiber optic sensors.

The emphasis in this project was a development of the nickel coating technology, including evaluating of the magnetic properties of the nickel coatings and some study of undercoating techniques. Some theoretical analysis was done. Coated fibers were delivered to the Naval Research Laboratory for test and evaluation of sensitivity, etc. in interferometric fiber optic sensor systems.

## **II. THEORETICAL ANALYSIS**

The basic structure to be considered for fabrication in this program involves a nickel layer plated on an underlayer of a different metal, on a glass fiber substrate. A theoretical analysis was made of the optical response to an acoustic/pressure input of such a two layer metal-coated optical fiber. This analysis serves to indicate the combinations of metal layer materials and thickness for which acoustic desensitization can be achieved.

To determine the expected range of magnetic sensitivity, an analysis was also made of the optical response of a fiber coated with a layer of magnetostrictive material.

These two analyses are contained in the following sections.

### **A. CALCULATIONS OF ACOUSTIC DESENSITIZATION OF TWO-LAYER METAL-COATED OPTICAL FIBER**

A previously published paper (1) analyzed the use for the fiber optic acoustic sensors of single-mode optical fibers coated with an elastic material. The result was a calculation of the pressure-induced optical phase shift for light traveling through such a fiber and the dependence of this phase shift on the elastic modulus, Poisson's ratio and thickness of the coating material.

Here we extend the analysis to the case of a fiber which has two concentric coatings of two different materials. The analysis is then

applied to the use of multi-layer metal coatings to obtain minimum acoustic sensitivity. The analysis follows the same steps as previous work. (1)

Consider the coated fiber shown in Fig. 1. The fiber is denoted as region 1 and is considered elastically homogeneous. It has radius  $R_1$ , Young's elastic modulus  $E_1$ , and Poisson's ratio  $\nu_1$ . It is coated with an inner layer of elastic material denoted as region 2, with a radius  $R_2$ , Young's modulus  $E_2$ , and Poisson's ratio  $\nu_2$ , and with an outer layer denoted as region 3, with a radius  $R_3$ , Young's modulus  $E_3$ , and Poisson's ratio  $\nu_3$ .

This composite structure is now placed under a uniform pressure  $P$ , and we will separately consider the radial, tangential, and axial components of the stresses, strains, and displacements in regions 1, 2, and 3. A set of linear equations we obtained in terms of the stress components by applying an appropriate set of boundary conditions, and these are solved numerically for various choices of the parameters  $R_i$ ,  $E_i$ ,  $\nu_i$  ( $i=1, 2, 3$ ).

Following References 1 and 2, we can set the stress components in cylindrical coordinates as follows:

$$\text{Radial Stress, } \sigma_r = \begin{cases} 2C_1 & \text{Region 1} \\ 2C_2 + A_2/r^2 & " 2 \\ 2C_3 + A_3/r^2 & " 3 \end{cases} \quad (1)$$

$$\text{Tangential Stress, } \sigma_\theta = \begin{cases} 2C_1 & \text{Region 1} \\ 2C_2 - A_2/r^2 & " 2 \\ 2C_3 - A_3/r^2 & " 3 \end{cases} \quad (2)$$

$$\text{Axial Stress, } \sigma_z = \begin{cases} F_1 & \text{Region 1} \\ F_2 & " 2 \\ F_3 & " 3 \end{cases} \quad (3)$$

The structure is considered to be long and thin ( $L \gg R_3$ ) so that, neglecting the small regions within a distance  $\sim R_3$  of the fiber ends by Saint-Venant's principle, (2) there can be no  $z$ -dependence of any stress or strain. The  $z$ -direction displacements must be equal in all three regions, linear with  $z$  and independent of  $r$  and  $\theta$ .

Now, the strains are given in general, by:

$$\epsilon_i = (1/E) [\sigma_i - \nu(\sigma_j + \sigma_k)] \quad (4)$$

where  $i, j, k = x, y, z$  or  $r, \theta, z$ . Therefore, the strains in radial and axial directions are:

Radial strain,  $\epsilon_r =$

$$\left. \begin{array}{l} (1/E_1) [2C_1(1-\nu_1) - \nu_1 F_1] \\ (1/E_2) [2C_2(1-\nu_2) - \nu_2 F_2] \\ \quad + (A_2/r^2)(1+\nu_2) \\ (1/E_3) [2C_3(1-\nu_3) - \nu_3 F_3] \\ \quad + (A_3/r^2)(1+\nu_3) \end{array} \right\} \begin{array}{l} \text{Region 1} \\ \text{"} \quad 2 \\ \text{"} \quad 3 \end{array} \quad (5)$$

$$\text{Axial strain, } \epsilon_z = \begin{cases} (1/E_1) [F_1 - 4v_1 C_1] & \text{Region 1} \\ (1/E_2) [F_2 - 4v_2 C_2] & " 2 \\ (1/E_3) [F_3 - 4v_3 C_3] & " 3 \end{cases} \quad (6)$$

The radial displacements  $u_r$  will also be required, where  $u_r = \epsilon_r d_r$ , so:

$$\text{Radial displacements, } u_r = \begin{cases} (1/E_1) [2C_1(1-v_1) - v_1 F_1] r & \text{Region 1} \\ (1/E_2) [2C_2(1-v_2) r - v_2 F_2 r \\ \quad - A_2(1+v_2)/r] & " 2 \\ (1/E_3) [2C_3(1-v_3) r - v_3 F_3 r \\ \quad - A_3(1+v_3)/r] & " 3 \end{cases} \quad (7)$$

There are 8 unknown constants -  $C_1, C_2, C_3, A_2, A_3, F_1, F_2, F_3$  - so that 8 boundary conditions are required. These can be stated as:

1. Radial stress at  $r=R_3$  equals the applied pressure.
2. Radial stress continuous at  $r=R_2$ .
3. Radial stress continuous at  $r=R_1$ .
4. Radial displacements equal at  $r=R_2$ .
5. Radial displacements equal at  $r=R_1$ .
6. Total axial force applied by the pressure equals the integrated axial stress.
7. Axial strains equal in regions 1 and 2 away from the ends.
8. Axial strains equal in regions 2 and 3 away from the ends.

Those boundary conditions can be written as:

$$1. \sigma_{r3}(R_3) = -P \quad (8a)$$

$$2. \sigma_{r3}(R_2) = \sigma_{r2}(R_2) \quad (8b)$$

$$3. \sigma_{r2}(R_1) = \sigma_{r1}(R_1) \quad (8c)$$

$$4. \quad u_{r3}(R_2) = u_{r2}(R_2) \quad (8d)$$

$$5. \quad u_{r2}(R_1) = u_{r1}(R_1) \quad (8e)$$

$$6. \quad -\pi R_3^2 P = \pi R_1^2 \sigma_{z1} + \pi (R_2^2 - R_1^2) \sigma_{z2} + \pi (R_3^2 - R_2^2) \sigma_{z3} \quad (8f)$$

$$7. \quad \epsilon_{z1} = \epsilon_{z2} \quad (8g)$$

$$8. \quad \epsilon_{z2} = \epsilon_{z3} \quad (8h)$$

where  $\sigma_{r2}$  designates the radial stress in regions 2, etc. These equations

(8a-h) can be written in terms of the constants A, C, F. as:

$$2C_3 + A_3/R_3^2 = -P \quad (9a)$$

$$2C_3 + A_3/R_2^2 = 2C_2 + A_2/R_2^2 \quad (9b)$$

$$2C_2 + A_2/R_1^2 = 2C_1 \quad (9c)$$

$$(1/E_3) [2C_3(1-v_3)R_2 - v_3 F_3 R_2 - A_3(1+v_3)R_2] = \quad (9d)$$

$$(1/E_2) [2C_2(1-v_2)R_2 - v_2 F_2 R_2 - A_2(1+v_2)/R_2] \quad$$

$$(1/E_2) [2C_2(1-v_2)R_1 - v_2 F_2 R_1 - A_2(1+v_2)/R_1] \quad$$

$$- (1/E_1) [2C_1(1-v_1)R_1 - v_1 F_1 R_1] \quad (9e)$$

$$-R_3^2 P = R_1^2 F_1 + (R_2^2 - R_1^2) F_2 + (R_3^2 - R_2^2) F_3 \quad (9f)$$

$$(1/E_1) [F_1 - 4v_1 C_1] = (1/E_2) [F_2 - 4v_2 C_2] \quad (9g)$$

$$(1/E_2) [F_2 - 4v_2 C_2] = (1/E_3) [F_3 - 4v_3 C_3] \quad (9h)$$

Changing variables to  $S=A_2/PR_2^2$ ,  $T=A_3/PR_3^2$ ,  $U=C_1/P$ ,  $V=C_2/P$ ,  $W=C_3/P$ ,

$X=F_1/P$ ,  $Y=F_2/P$ , and  $Z=F_3/P$  and designating the ratios  $E_2/E_1 = E_{21}$ ,  $E_{31} = E_3/E_1$ ,

$R_{32} = R_3/R_2$  and  $R_{21} = R_2/R_1$ , we can write these equations in matrix form as



Thus we have eight linear equations in terms of the eight constants which determine the stresses in Eqs. (1) - (3), and from which the strains and displacements can be determined using Eqs. (5) - (7). All of those relationships are now expressed in terms of the the material parameters  $E_{32}$ ,  $E_{21}$ ,  $R_{32}$ ,  $R_{21}$ ,  $v_1$ ,  $v_2$  and  $v_3$ , and all are linear in pressure  $P$ .

Following Ref. 1, we write the optical phase shift  $\Delta\phi$  induced by a pressure  $P$  in a fiber length  $L$  as:

$$\Delta\phi = \beta \epsilon_{21} L - \frac{1}{2} L \beta n^2 \Delta(1/n^2) \quad (11)$$

where the change in the optical indicatrix is:

$$\Delta(1/n^2) = (P_{11} + P_{12}) \epsilon_{r1} + P_{12} \epsilon_{z1} \quad (12)$$

and  $\beta$  is the optical propagation constant,  $n$  the index of refraction, and  $P_{11}$  and  $P_{12}$  the strain-optic coefficients. The normalized pressure-induced optical phase shift therefore is:

$$\frac{\Delta\phi}{P} \frac{E_1}{8L} = X \left( 1 + (n^2/2) \right) \left[ (P_{11} + P_{12}) v_1 - P_{12} \right] + U \left[ -4v_1 - n^2 \left[ (P_{11} + P_{12})(1 - v_1) - 2v_1 P_{12} \right] \right] \quad (13)$$

The usual material for single-mode fiber is fused silica, for which  $n=1.456$ ,  $P_{11}=0.121$ ,  $P_{12}=0.270$ ,  $E=7 \times 10^{12}$  Pa, and  $v=0.17$ . Thus we have:

$$\frac{\Delta\phi}{P} \frac{E_1}{8L} = 0.7843X - 1.1734U \quad (14)$$

We have calculated numerically the solutions to Eq. (10), and from them the phase shift (14) for fibers with the outer coating (region 3) of nickel and with the inner coating (region 2) of copper and of aluminum. These devices correspond to the materials used in the present project, which emphasizes the use of electroplated nickel for magnetic sensitivity and for acoustic desensitization. Using the calculations of Ref. 1 for single-layer coated fibers, nickel coating is found to decrease the acoustic sensitivity to zero for relatively thin coatings - approximately 10% of the fiber diameter.

For nickel, we assume  $v_3 = 0.336$  and  $E_3 = 21.4 \times 10^{10}$  Pa, so  $E_{31} = 3.057$ . For copper,  $v_2 = 0.37$  and  $E_{21} = 1.714$ , while for aluminum,  $v_2 = 0.33$  and  $E_{21} = 1.000$ .

Results for the normalized pressure-induced phase shift  $(\Delta\phi/P)/(E_1/\beta L)$  plotted versus normalized nickel thickness  $R_{32}$  for various choices of normalized copper undercoating thickness  $R_{21}$  are shown in Figure 2. Similar results are given in Figure 3 for a nickel outer coating and an aluminum inner coating. In each figure, the curve for zero undercoating thickness ( $R_{21} = 0$ ) is also plotted. For comparison, note that for an uncoated fiber,  $(\Delta\phi P)/E_1/\beta L = -0.198$ .

In all cases, desensitization of the fiber to pressure-induced effects can be achieved at a particular Ni coating thickness. With thicker undercoating, less Ni is required, and this effect is greater for Cu undercoating than for Al. For a fiber of diameter 100  $\mu$ m ( $k_1 = 50 \mu\text{m}$ ), the required Ni thickness ranges from 10.6  $\mu\text{m}$  with no undercoating to a thickness of only a few  $\mu\text{m}$  for thicker Cu undercoating. To achieve a factor of ten reductions in acoustic sensitivity, the tolerance on the Ni coating thickness is approximately  $\pm 30\%$ .

The values of  $v_3$  and  $E_3$  for both nickel and the undercoating as deposited on the fiber may vary from the bulk values used above. In this case, experimental results of acoustic sensitivity in coated fibers can be used to correct these values and to predict optimized

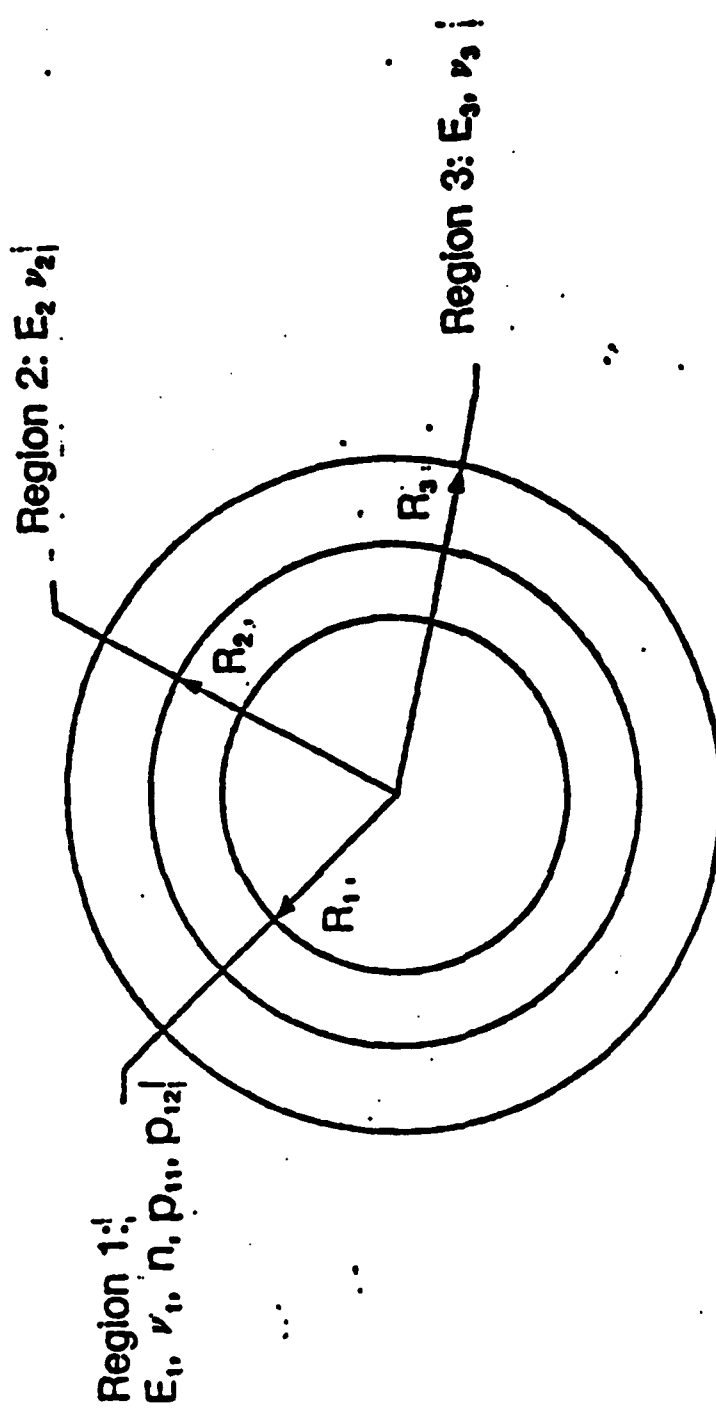
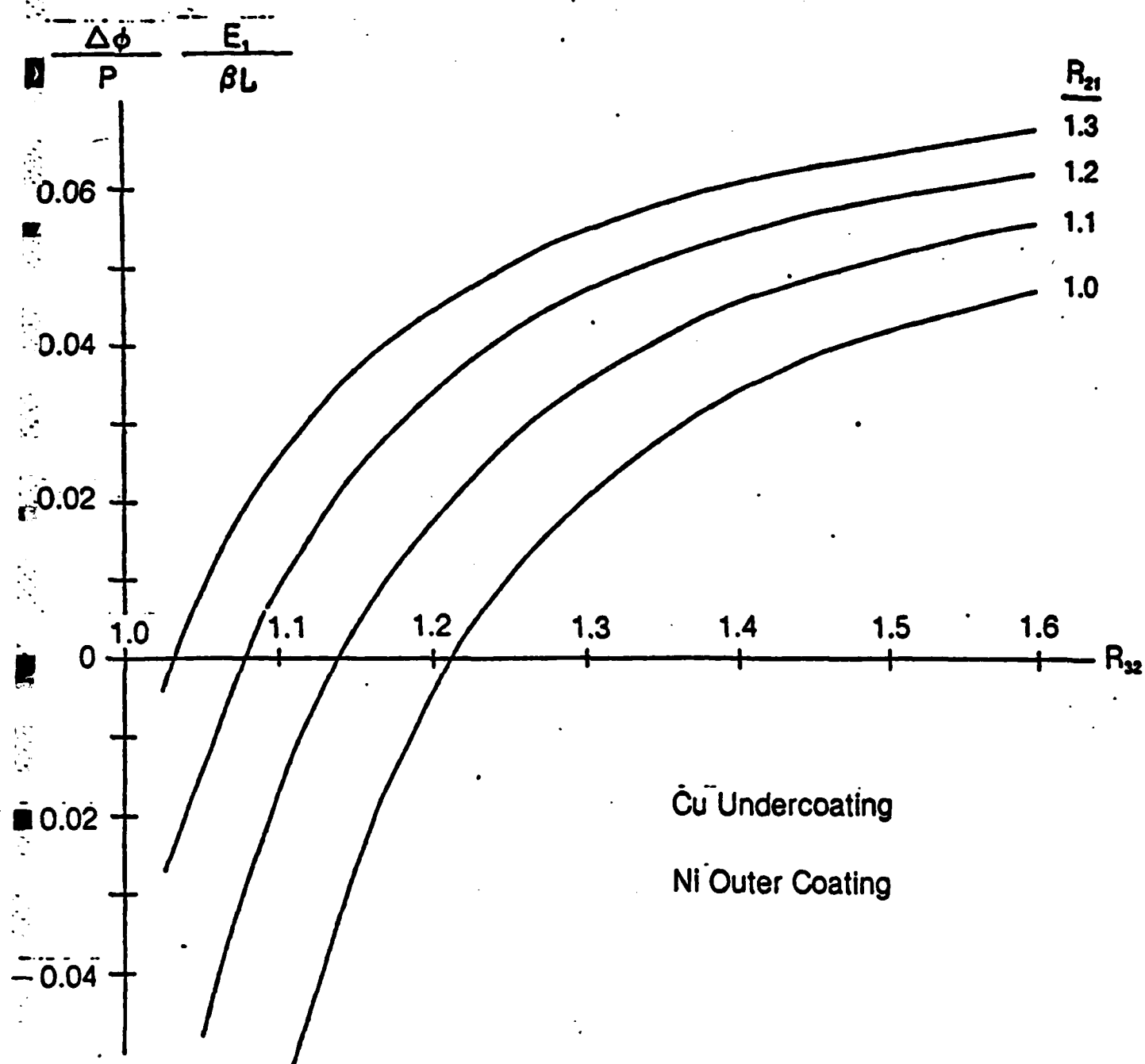
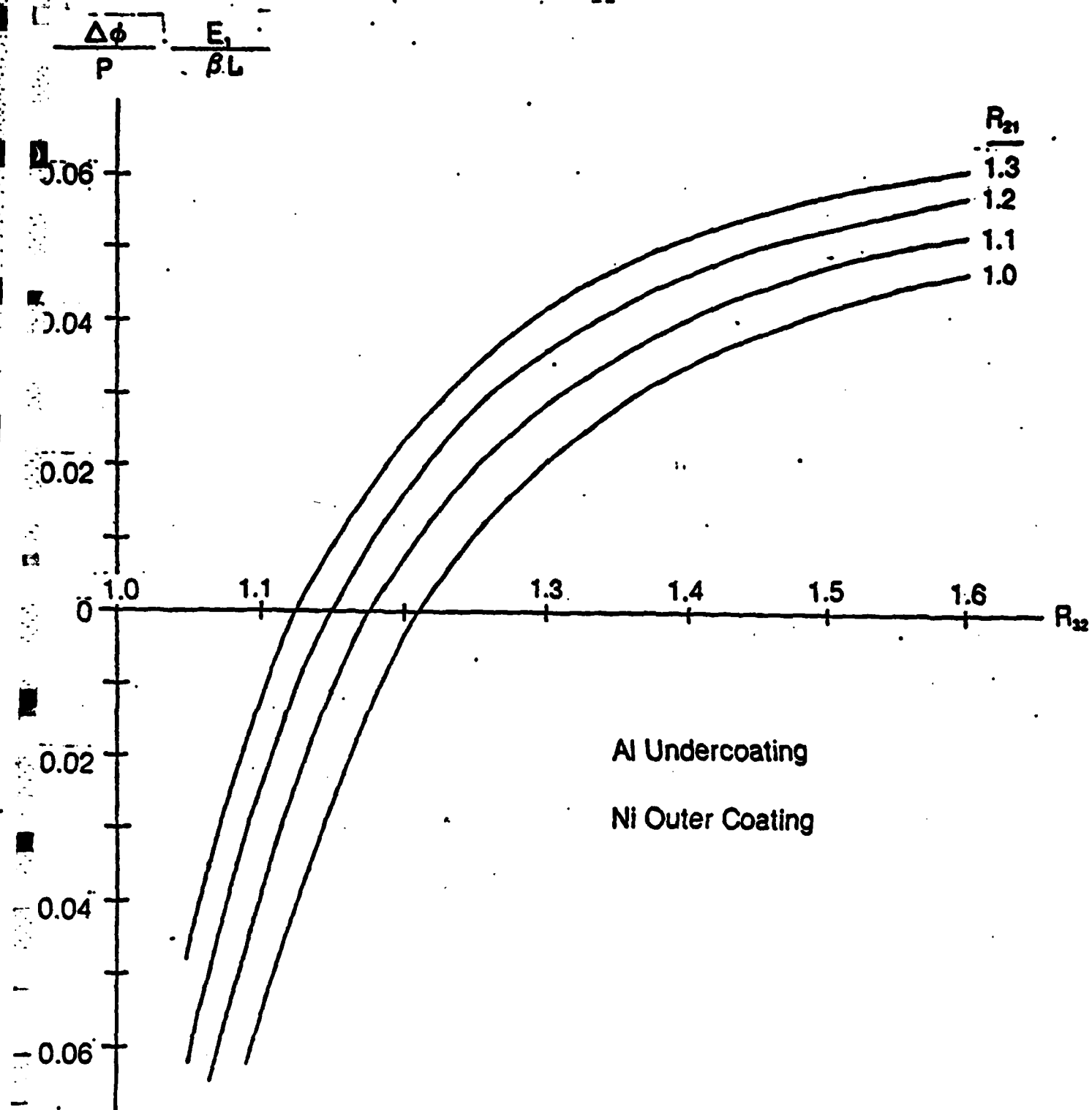


Figure 1: Cross section of optical fiber (region 1) coated with inner coating (region 2) and outer coating (region 3). The fiber has Young's modulus  $E_1$ , Poisson's ratio  $\nu_1$ , index of refraction  $n$ , and strain-optic coefficients  $\rho_{11}$  and  $\rho_{12}$ . The inner and outer coatings have Young's modulus  $E_2$  and  $E_3$ , and Poisson's ratio  $\nu_2$  and  $\nu_3$ , respectively.



**Figure 2.** Normalized pressure-induced phase shift versus normalized nickel outer coating thickness for copper undercoated fiber.



**Figure 3.** Normalized pressure-induced phase shift versus normalized nickel outer coating thickness for aluminum undercoated fiber.

## B. ANALYSIS OF MAGNETIC SENSITIVITY OF OPTICAL FIBER COATED WITH MAGNETOSTRICTIVE MATERIAL

It has been suggested (3) and demonstrated (4) that the use of single-mode fibers coated with magnetostrictive material can lead to sensitive, fiber-optic magnetometers. In this analysis, we adapt the previous analysis (1) to the case of a magnetostrictive coated fiber and its response to an axial magnetic field. The magnetically-induced optical phase shift in light traveling through the fiber will be calculated as a function of the elastic properties of fiber and coating, the magnetostrictive properties of the coating, the optical and elasto-optic properties of the fiber, and of the relative dimensions.

A cross-section of the coated fiber is shown in Figure 4. The fiber (region 1) has radius  $R_1$ , Young's elastic modulus  $E_1$ , Poisson's ratio  $\nu_1$ , optical index of refraction  $n$ , and strain-optic coefficients  $p_{11}$  and  $p_{12}$ . The magnetostrictive coating material (region 2) has elastic modulus  $E_2$ , Poisson's ratio  $\nu_2$ , and piezomagnetic strain constant  $d$ .

It is assumed that a static magnetic bias field is applied, determining the value of  $d$ , and that the perturbations about that operating point due to some incremental axial field  $H$  are to be calculated. The general relationship between stress ( $\sigma$ ) and strain ( $\epsilon$ ), including magnetostriction, can be written as:

$$\epsilon = d \cdot H + \sigma/E \quad (15)$$

Using cylindrical coordinates and following the analysis of Ref. 1, the stress in regions 1 and 2 can be written as:

$$\sigma = \begin{cases} A/r^2 + 2C & \text{Region 2} \\ 2D & \text{Region 1} \end{cases} \quad (16)$$

$$\sigma_0 = \begin{cases} -A/r^2 + 2C \\ 2D \end{cases} \quad \begin{matrix} \text{Region 2} \\ \text{Region 1} \end{matrix} \quad (17)$$

$$\sigma_z = \begin{cases} F \\ G \end{cases} \quad \begin{matrix} \text{Region 2} \\ \text{Region 1} \end{matrix} \quad (18)$$

In magnetostrictive materials, we have additional strain terms due to magnetostriction, so that:

$$\epsilon_1 = (1/E) [\sigma_i - v(\sigma_j + \sigma_k)] + dH_1 - d(H_j + H_k)/2 \quad (19)$$

where we have assumed zero volume magnetostriction (giving the factors of 1/2 in the last term) and where  $d$  depends on the biased operating point on the  $E$  vs.  $H$  curve, while  $H$  is the incremental change from that operating point. The strains can be written:

$$\epsilon_r = \begin{cases} (1/E_1) [2D(1-v_1) - v_1 G] \\ (1/E_2) [A(1+v_2)/r^2 + 2C(1-v_2) - v_2 F] \end{cases} - dH_z/2 \quad \begin{matrix} \text{Region 1} \\ \text{Region 2} \end{matrix} \quad (20)$$

$$\epsilon_z = \begin{cases} (1/E_1)(G - 4v_1 D) \\ (1/E_2)(F - 4v_2 C) \end{cases} + dH_z \quad \begin{matrix} \text{Region 1} \\ \text{Region 2} \end{matrix} \quad (21)$$

It will also be required to express the radial displacements in terms of the same quantities.

$$u_r = \begin{cases} (1/E_1) [2D(1-v_1) - v_1 G] r \\ (1/E_2) [-A(1+v_2)/r + 2C(1-v_2) r - v_2 F r] - dH_z r/2 \end{cases} \quad \begin{matrix} \text{Region 1} \\ \text{Region 2} \end{matrix} \quad (22)$$

The stresses, strains and displacements we all expressed in terms of the five constants A, C, D, F, and G. Thus, five boundary conditions are required to give the necessary relationships to solve for these constants. The boundary conditions are:

1. No radial stress at outside ( $r = R_2$ )
2. Radial stresses in regions 1 and 2 equal at boundary ( $r = R_1$ )
3. Radial displacements in regions 1 and 2 equal at boundary ( $r = R_1$ )
4. Net axial force is zero
5. Equal axial strains in regions 1 and 2 (away from ends)

Mathematically, these we express as:

$$1. \sigma_{r2}(R_2) = 0 \rightarrow \frac{A}{R_2^2} + 2C = 0$$

$$2. \sigma_{r1}(R_1) = \sigma_{r2}(R_1) \rightarrow \frac{A}{R_1^2} + 2C = 2D$$

$$3. u_{r1}(R_1) = u_{r2}(R_1) \rightarrow$$

$$\frac{1}{E_1} \left[ 2D(1-v_1) - v_1 G \right] R_1 = \frac{1}{E_2} \left[ -\frac{(1+v_2)}{R_1} A + 2C(1-v_2)R_1 - v_2 F R_1 \right]$$

$$\therefore \frac{1}{2} \frac{d}{4\pi} H_2 R_1$$

$$4. \pi R_1^2 \sigma_{z1} + \pi (R_2^2 - R_1^2) \sigma_{z2} = 0 \Rightarrow R_1^2 G + (R_2^2 - R_1^2) F = 0$$

$$5. \epsilon_{z1} = \epsilon_{z2} \Rightarrow \frac{1}{E_1} (G - 4v_1 D) = \frac{1}{E_2} (F - 4v_2 C) + \frac{d}{4\pi} H_2$$

To normalize, we change variables to:

$$X = \frac{A}{E_1 R_2^2 \frac{d}{4\pi} H_2}$$

$$Z = \frac{ZD}{E_1 \frac{d}{4\pi} H_2}$$

$$W = \frac{C}{E_1 \frac{d}{4\pi} H_2}$$

$$Y = \frac{2C}{E_1 \frac{d}{4\pi} H_2}$$

$$V = \frac{F}{E_1 \frac{d}{4\pi} H_2}$$

and use the ratios:

$$R = R_2/R_1$$

$$E = E_1/E_2$$

resulting in the matrix equation:

$$\begin{bmatrix} 1 & 1 & 0 & 0 & 0 \\ R^2 & 1 & -1 & 0 & 0 \\ (1+v_2) ER^2 & -(1-v_2)E & (1-v_1) v_2 E & -v_1 & \\ 0 & 0 & 0 & (R^2-1) & 1 \\ 0 & 2 v_2 E & -2v_1 & -E & 1 \end{bmatrix} \begin{bmatrix} X \\ Y \\ Z \\ V \\ W \end{bmatrix} = \begin{bmatrix} 0 \\ 0 \\ -1/2 \\ 0 \\ 1 \end{bmatrix} \quad (23)$$

Now, the optical phase shift in a length L of fiber for light with propagation constant of is:

$$\begin{aligned} \Delta\phi &= \beta\epsilon_{z1} L + \Delta\phi_{AB} \\ &= \beta\epsilon_{z1} L - 1/2 LB n^2 \Delta \left( \frac{1}{n^2} \right)_{x,y} \end{aligned} \quad (24)$$

Where the change in the optical indicatrix is

$$\Delta \left( \frac{1}{n^2} \right)_{x,y} = (P_{11} + P_{12}) e_{y1} + P_{12} e_{z1} \quad (25)$$

Expressing (24) and (25) in terms of the parameters  $X, Y, Z, V, W$  and carrying out some algebraic manipulation, results in an expression for the normalized optical phase shift per unit fiber length per unit magnetic field change:

$$\frac{\frac{d\phi}{dH_2}}{4\pi BL} = W \left[ 1 + \frac{1}{2} n^2 v_1 (P_{11} + P_{12}) \right] - \frac{1}{2} n^2 P_{12} \quad (26)$$

$$+ Z \left[ -2v_1 - \frac{1}{2} n^2 (P_{11} + P_{12}) (1 - v_1) + n^2 P_{12} v_1 \right]$$

Since to calculate the response given by (26) from (23) we only need  $Z$  and  $W$ , we can simplify (23) to only contain  $Z$  and  $W$ :

$$\begin{bmatrix} \frac{E}{R^2-1} & \left[ (1+v_2) R^2 + (1-v_2) \right] + (1-v_1) & \frac{-v_2 E}{R^2-1} & -v_1 \\ & -2v_1 - \frac{2v_2 E}{R^2-1} & & \\ & & 1 + \frac{E}{R^2-1} & \end{bmatrix} \begin{bmatrix} Z \\ W \end{bmatrix} \cdot \begin{bmatrix} \frac{1}{Z} \\ 1 \end{bmatrix} \quad (27)$$

If we assume that the fiber is fused silica and the coating is nickel, then:

$$n = 1.456$$

$$P_{11} = 0.21$$

$$P_{12} = 0.27$$

$$v_1 = 0.17$$

$$v_2 = 0.336$$

$$E = E_1 / E_2 = \frac{7 \times 10^{10} \text{ Pa}}{21.4 \times 10^{10} \text{ Pa}} = 0.327$$

The normalized phase shift resulting when those values are used in (27) is plotted in Figure 5 versus radius ratio R. We can also calculate the asymptote as  $R \rightarrow 00$  as:

$$\left. \frac{\Delta\phi}{\frac{d}{\pi} H_z B L} \right|_{\text{max.}} = 1.2122$$

From Figure 5 we see that the normalized magnetically-induced optical phase achieves 1/2 its maximum value for  $R = 1.18$ . For a 100  $\mu\text{m}$  O.D. fiber this corresponds to a nickel coating of  $18 \mu\text{m}$  thickness. If, for Ni,  $d = 39 \times 10^{-7} \text{ G}^{-1}$ , then for a He-Ne laser with  $\lambda = 0.6328 \mu\text{m}$  max. we find the maximum magnetic sensitivity can be calculated to be:

$$\left. \frac{\Delta\phi}{H_z L} \right|_{\text{max.}} = 4.49 \text{ rad/G-m}$$

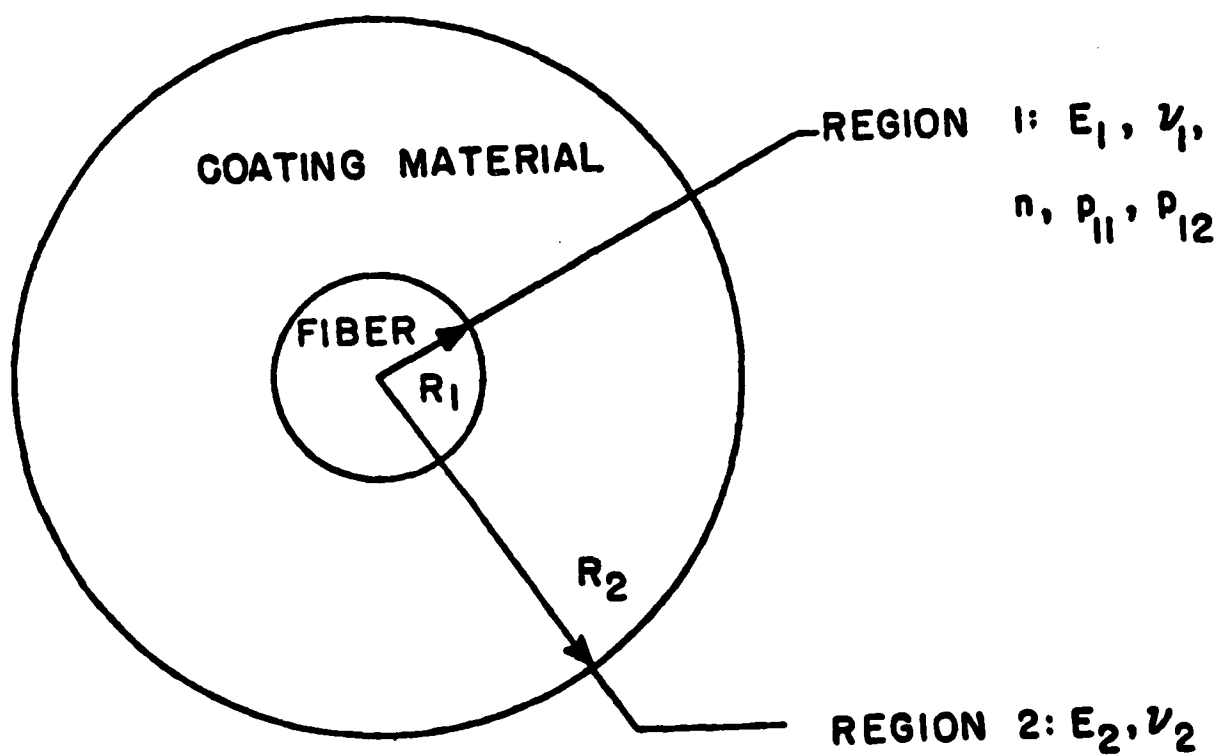


Figure 4. Cross section of optical fiber (region 1) coated magnetostriuctive material (region 2). The fiber has Young's modulus  $E_1$ , Poisson's ratio  $\nu_1$ , index of refraction  $n$ , and strain-optics coefficients  $p_{11}$  and  $p_{12}$ . The coating has Young's modulus  $E_2$  and Poisson's ratio  $\nu_2$ .

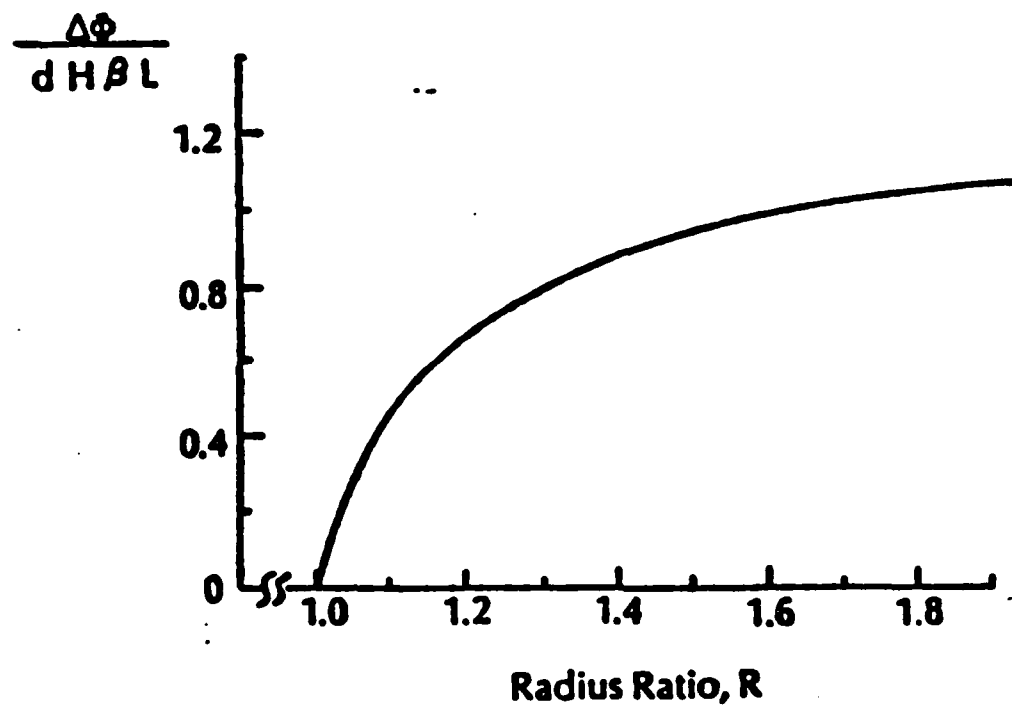


Figure 5. Normalized magnetostriuctive-induced optical phase shift versus radius ratio.

### III. UNDERCOATINGS

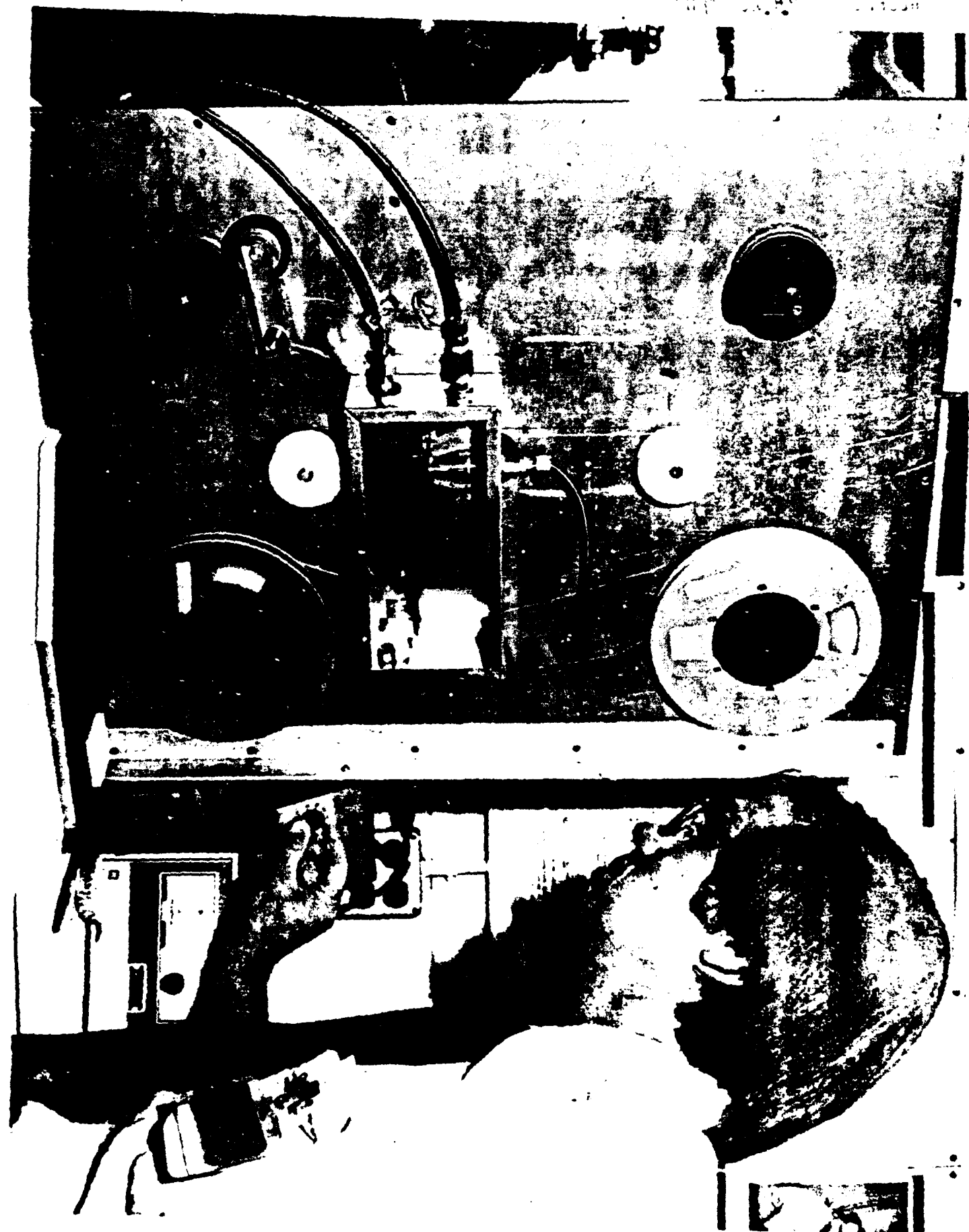
In order to electroplate Ni onto the fibers, it is first required to apply a conductive undercoating, showing good adhesion and the ability to withstand subsequent annealing steps, if any. Three methods were investigated: Freeze coating of relatively low melting point metals, sputtering, and electroless deposition. They are described in subsequent sections.

#### A. FREEZE COATING

Early in this program, the freeze coating method (5,6) was utilized for some lower melting temperature metals and alloys. These included indium, tin, zinc, and aluminum as well as some alloys of the first three. A photograph of the equipment used is shown in Fig. 6. Glass fiber was first stripped of its factory-applied polymer coating, cleaned, and then pulled through a crucible of the molten metal by the arrangement of reels and rollers shown. The temperature of the molten metal and the fiber pull speed could both be adjusted for optimum results. The freeze-coating process has the advantage that it is a continuous line process, able to be scaled to fibers of arbitrarily long length.

Indium and zinc provided the best coatings, but it was difficult to obtain uniformly coated layers, even with these. In fact, an underlayer should be applied when the fiber is in its pristine state, so it would be best if this conductive underlayer were applied as the fiber is pulled, i.e. by the fiber manufacturer. Since we were required to strip off the polymer coatings already applied, using a combination of chemical and mechanical means, imperfect surface cleanliness and possibly surface damage are believed to be the source of the problems encountered with coating adhesion and uniformity.

Because of these difficulties with freeze coating as a means to apply undercoating, it was decided not to proceed with this side issue, but



rather to concentrate on the nickel electroplating process. As described in the next section, an RF sputter deposition technique was found to be adequate for undercoating the relatively short lengths of fibers required by this work.

**B. SPUTTER DEPOSITION**

RF sputter deposition is commonly used at Honeywell to deposit metal layers in the fabrication of semiconductor circuits, thin-film packages, and miniature sensors. This technique was applied to undercoating of optical fibers and gave excellent, adhesive undercoatings of metals which could withstand later annealing. Underlayers are applied by first stripping a length of fiber (up to 5 meters) of its jacket and coatings, cleaning, and loosely coiling on the rotating table in a Veeco 2400 RF sputtering system. Two depositions are required to coat the entire periphery of the fiber, with the fiber being turned over between depositions. Underlayer coatings consisting of 500 Å of chrome followed by 4000 Å of copper were used for all subsequent work, including all fibers delivered to NRL.

**C. ELECTROLESS NICKEL DEPOSITION**

A process was identified to pre-treat glass to permit direct electroless deposition of Ni. Electroless Ni deposition was previously considered in the Honeywell-funded program during 1980, but was abandoned because electroless Ni is not ferromagnetic (due to the presence of phosphorus impurities) and because attempts to deposit on glass were unsuccessful. However, since conductive undercoating materials which withstand annealing are a major problem, we attempted to apply a thin layer of electroless Ni and then to electroplate a thick layer of pure Ni, thus allowing subsequent annealing.

Samples of fiber and cover slips were plated with 0.3 µm electroless Ni using a proprietary process by the Honeywell Defense Systems Division. Such films are smooth, continuous, and show good adhesion.

The electroless Ni takes only several minutes to deposit and appears compatible with a continuous line coating process. Efforts to electroplate thick, pure Ni onto these electroless undercoatings were successful. However, the electroless Ni film loses adhesion with the fiber at temperatures about 500°C, and also was found to seriously degrade the fiber strength. We conclude that this process does not solve the problem of obtaining a suitable undercoating, and that such an undercoating is still best applied at the time the fiber is drawn.

#### IV. NICKEL-ELECTROPLATING

##### A. PLATING BATHS

The most commonly used nickel plating bath formulation is called the watts bath. Its primary source of nickel is nickel sulfate ( $\text{NiSO}_4$ ). Initially we used the watts bath but later switched to a nickel sulfamate ( $\text{Ni}(\text{NH}_2\text{SO}_3)_2$ ) bath because it can produce deposits of lower stress and can be used at higher plating rates. A low stress deposit is desirable since the magnetic properties are enhanced. The makeup of a nickel sulfamate bath is listed in Table I. The brightening agent PCB4 is optional, but was included in the plating bath in most cases because of the improvement in film brightness and reduced stress.

TABLE I

COMPOSITION OF NICKEL SULFAMATE PLATING BATH

BATH INGREDIENTS	AMOUNT PER LITER OF SOLUTION
Nickel Sulfamate Concentrate*	470.0 ml
Nickel Bromide Solution*	47.4 ml
Boric Acid	28.2 g
Deionized Water	432.3 ml
PCB 4 **+	38.0 ml

\*Available from Harstan Chemical Corporation, Brooklyn, NY

\*\*PCB4 is a deposit modifier which is said to reduce stress in the deposit, make it harder and produce a bright deposit.

#### B. NICKEL ON PLANAR SUBSTRATES

Planar substrates were used to test plating baths and determine the quality of deposits made from them prior to plating fiber. Microscope cover slips made from both glass and quartz, 18 mm square, were sputtered with chrome and copper and subsequently nickel plated. B-H loops were made to determine coercivity (Hc) and loop squareness of the plated nickel. Magnetostriiction measurements were done using facilities at the University of Minnesota. These tests will be described in later sections.

#### C. NICKEL PLATING ON OPTICAL FIBERS

System Description - Attempts to plate nickel on undercoated fiber in a heater in a batch mode were unsatisfactory because the resulting nickel coating was not uniform in thickness. We thus moved to plating of fiber in a continuous mode sooner than anticipated. We utilized available plating cells from work previously done for plated wire memory. The plated wire memory was initially developed here (7,8) and is currently being produced at Honeywell's Clearwater, Florida, location. These cells were adapted to plate nickel on suitable undercoated fiber. A schematic representation of the continuous fiber plating process is shown in Figure 7. A continuously-circulating, temperature-controlled plating bath is utilized. The cells have multiple passages to ensure circulation of fresh plating solution around the fibers for maximum uniformity.

Either a mercury contact or a rolling metal cylinder was used to transfer current from the power supply to the fiber. Nickel anodes inserted in the plating cells were used to complete the circuit from

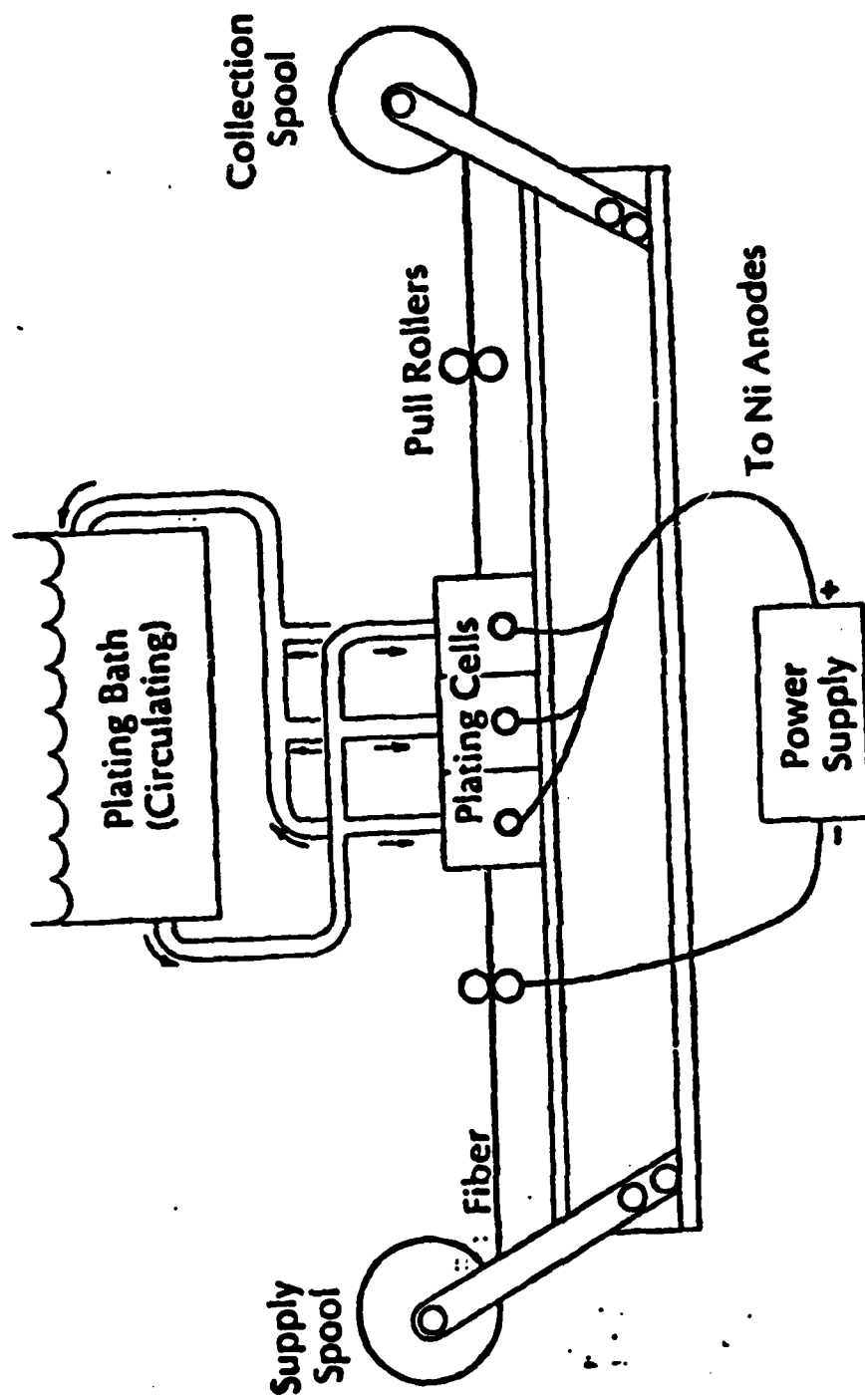


Figure 7. Continuous fiber plating line.

the plating solution back to the power supply. A four liter beaker was used as a reservoir for the plating bath. Plating solution from the reservoir flows thru tygon tubing to a pump which forces the solution thru the cells and back to the reservoir. The fiber is pulled thru the plating cells at a constant rate and wound upon a reel. Nickel thickness is controlled by adjusting the velocity of the fiber and by adjusting the current. A typical current density in each of the four plating cells is  $450 \text{ mA/cm}^2$  and a typical fiber velocity is  $4 \text{ cm/min}$ . These conditions yield a nickel coating of about  $15\mu\text{m}$  on fiber initially  $86 \mu\text{m}$  in diameter.

#### **D. PLATING OF ALUMINUM-UNDERCOATED FIBERS**

Fibers undercoated with aluminum by freeze coating at the time the fiber was pulled were supplied by NRL for subsequent Ni plating. Some initial difficulty was experienced in trying to plate on aluminum. A process called zinc immersion (9) was found necessary to prepare the aluminum surface for nickel plating. It was also discovered that the roller contact method to transfer current to the fiber was necessary when plating because the zinc on the "zincated" aluminum reacts and forms an amalgam with the mercury when using the mercury contact technique. Using those techniques, good electroplated Ni coatings were obtained on these fibers.

#### **V. ANNEALING**

The magnetostrictive behavior of a nickel film is critically dependent upon its internal stress state. This in turn is a function of deposition conditions such as plating bath composition, current, temperature, etc., and of subsequent processing such as annealing. Achieving a high slope for the magnetostrictive strain versus magnetic field curve requires a low-stress deposit. For those reasons, the effects of annealing on nickel coated fibers prepared for magnetic field sensing were investigated as a part of this program.

Annealing was carried out in a small tube furnace equipped with

flowing gas capabilities. The furnace itself was 50 cm long, and the system could accomodate fibers up to 1.1m length. Only the central part in the furnace was annealed. Typically, after the fiber(s) was inserted, the tube was flushed with  $N_2$  followed by  $H_2$ , and a slow  $H_2$  flow was continued throughout annealing.

The first annealed fiber (Delivered 4/8/81, See Table V) was heated and cooled at about  $15^{\circ}C/min.$  and was held at  $950^{\circ}C$  for 1 hour.

Later, an effort was made to reduce strains caused by differential thermal expansion between fiber and coating by (a) heating and cooling at slower rates and (b) annealing at lower temperatures for longer times. The fibers delivered on 9/24/81 (See Table V) were heated and cooled at 1 to  $1.5^{\circ}C/min.$  and held at maximum temperature for  $\sim 12$  hours. Maximum temperature of  $400^{\circ}C$ ,  $600^{\circ}C$ , and  $950^{\circ}C$  were employed.

Samples of electroplated Ni films on planar substrates were also annealed to study the effects on magnetostriction, B-H loops, etc. The same furnace and procedures were employed. Results are summarized in Section VII.

## **VI. TEST PROCEDURES**

Tests of acoustic or magnetic sensitivity of the coated fibers in an interferometric optical sensor system were carried out at NRL on fibers delivered under this contract and will not be reported on here. Two tests of magnetic characteristics of plated nickel films were performed under this contract: B-H loop measurements and measurements of the magnetostrictive strain versus field. These test procedures are described below, and results are given in Section VII.

### **A. B-H LOOPS**

Measurements of B-H hysteresis loop characteristics of electroplated nickel films on planar substrates and on fibers were carried out on equipment developed for that purpose at Honeywell as a part of past

programs on thin-film magnetic materials. The method of operation of this B-H looper is as follows: An AC magnetic field is created by a pair of field coils. There are a pair of pick-up coils called the bucking coil and the sample coil, which are oppositely wound so that, with no sample in place, the signals induced by the AC field cancel. When the sample is placed in the sample coil, this balance is upset by the amount of flux due to the sample. The inductive output  $d\phi/dt$  is electronically integrated to give flux  $\phi$  , proportional to B in the sample.

An x-y plot of H applied versus B sample is displayed on an oscilloscope, tracing the desired hysteresis loop of the sample. While the H values resulting from the applied field are easily calibrated, calibration of the B-axis is more difficult. For planar thin-film samples, approximate calibration is possible using secondary thin-film standards if the sample thickness and width are known. For more complex sample geometry such as plated fibers, B-axis calibration is not possible.

#### **B. MAGNETOSTRICTION MEASUREMENTS**

Magnetostriction measurements were performed on planar substrates at the University of Minnesota. Professor William Robbins of the Department of Electrical Engineering has set up a system in which the planar magnetic samples form half of a capacitor. Under influence of a magnetic field, the magnetostrictive coating on a substrate will cause the cantilevered sample to bend slightly and change the capacitance. By accurately measuring the capacitance and the capacitance change plus knowing certain constants of the film and substrate, magnetostriction of the material can be calculated. This method is shown in Fig. 8.

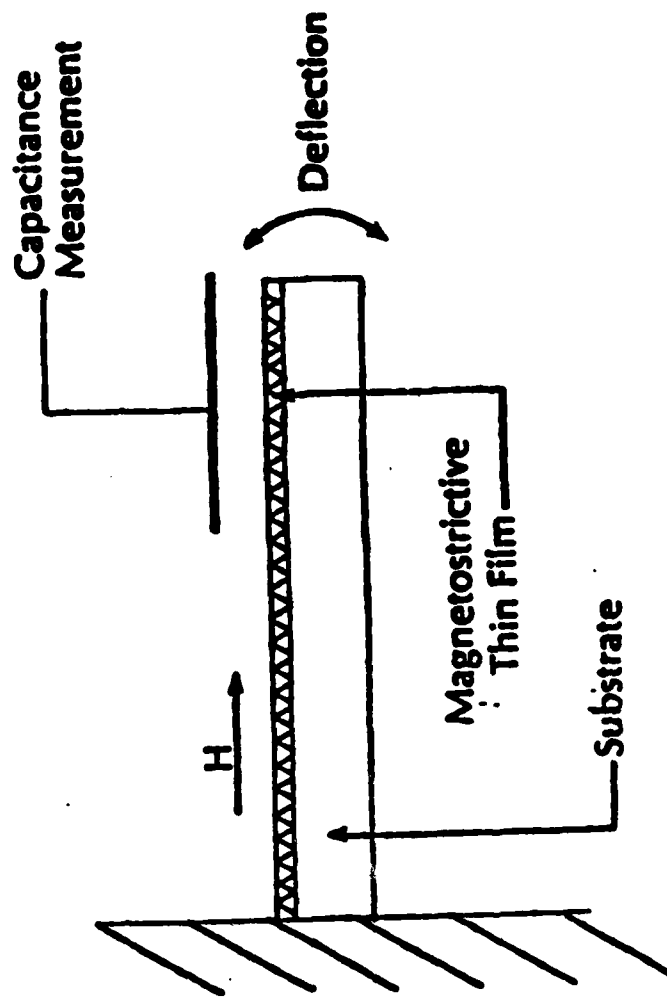


Figure 8. Method of measuring magnetostriction in thin-film sample on planar substrate.

## VII. TEST RESULTS

### A. B-H LOOP DATA

Table II summarizes some of the data on B-H loop measurements made on planar substrates plated from different baths. The general results are that (a) the nickel deposited from the sulfamate bath with the deposit modifier PCB 4 has a lower unannealed coercivity than the nickel deposited from a watts bath, and (b) the B-H loop is much more square than that from a watts bath deposit.

Results of sulfamate bath plated nickel deposits annealed at different temperatures are also shown in Table II. The conclusion here is that although annealing of these samples lowered coercivity with increased anneal temperature, at the same time the loop squareness decreased. For magnetometer purposes, low coercivity deposits are highly desired but the importance of loop squareness is unclear.

B-H loop measurements also were performed on small segments of fiber, both annealed and not annealed. The results are shown on Table III along with corresponding results from planar substrates. For both planar and fiber substrates, coercivity dropped upon annealing at 950°C. However, for planar substrates the loop was initially fairly square and upon annealing it was not nearly as square. The result for plated fiber was opposite: unannealed fiber loop initially was not square but became square upon annealing. Both annealed samples (planar and fiber) exhibited the cracked appearance in the nickel. The loop squareness difference between planar and fiber samples is perhaps related to the relative amounts of nickel making up the sample or to substrate geometry.

TABLE II: RESULTS FOR PLANAR SUBSTRATES, PLATED FROM  
WATTS AND SULFAMATE BATHS

BATH	ANNEAL STATUS	COERCIVITY	LOOP SQUARENESS (Br/Bm) x 100%
Watts	Not annealed	58	50
Sulfamate with PCB 4	Not annealed	39.1	90
Sulfamate with PCB 4	Annealed 600 C	17.4	56.8
Sulfamate with PCB 4	Annealed 950 C	13.0	40.4

TABLE III: RESULTS COMPARED FOR FIBERS AND  
PLANAR SUBSTRATES, PLATED FROM SULFAMATE BATH

SUBSTRATE	ANNEAL STATUS	COERCIVITY (Oe)	LOOP SQUARENESS (Br/Bm) x 100%
Planar-Quartz	Not annealed	39.1	90.9
Planar-Quartz	Annealed 950 C	13.0	40.4
Fiber	Not annealed	34.8	17
Fiber	Annealed 950 C	11.0	90

**B. MAGNETOSTRICTION MEASUREMENT ON PLANAR SUBSTRATES**

A magnetic field sensor should have high response to small changes in magnetic field, i.e. the slope of the magnetostriction -vs- magnetic field curve should be maximized. Typical results are shown in Figures 9, 10, and 11. Table IV summarizes some of the data obtained from tests at the University of Minnesota. It appears that 950°C annealed samples performed better than the corresponding unannealed samples. Also, nickel plated from a sulfamate bath with PCB 4 responded better than nickel from a watts bath. This can be attributed to lower stress in the deposit. The most important results are those obtained in a fiber optic interferometer configuration. These will be obtained at NRL from fiber samples delivered.

TABLE IV: MAGNETOSTRICTION MEASUREMENT RESULTS ON PLANAR SUBSTRATES

BATH	ANNEAL STATUS	SLOPE OF STRAIN VS. FIELD CURVE (G <sup>-1</sup> )
Watts	Not annealed	0.028 x 10 <sup>-6</sup>
Watts	Annealed 950 C	0.053 x 10 <sup>-6</sup>
Sulfamate	Not annealed	0.050 x 10 <sup>-6</sup>
Sulfamate with PCB 4	Not annealed	0.084 x 10 <sup>-6</sup>
Sulfamate with PCB 4	Annealed 950 C	0.099 x 10 <sup>-6</sup>

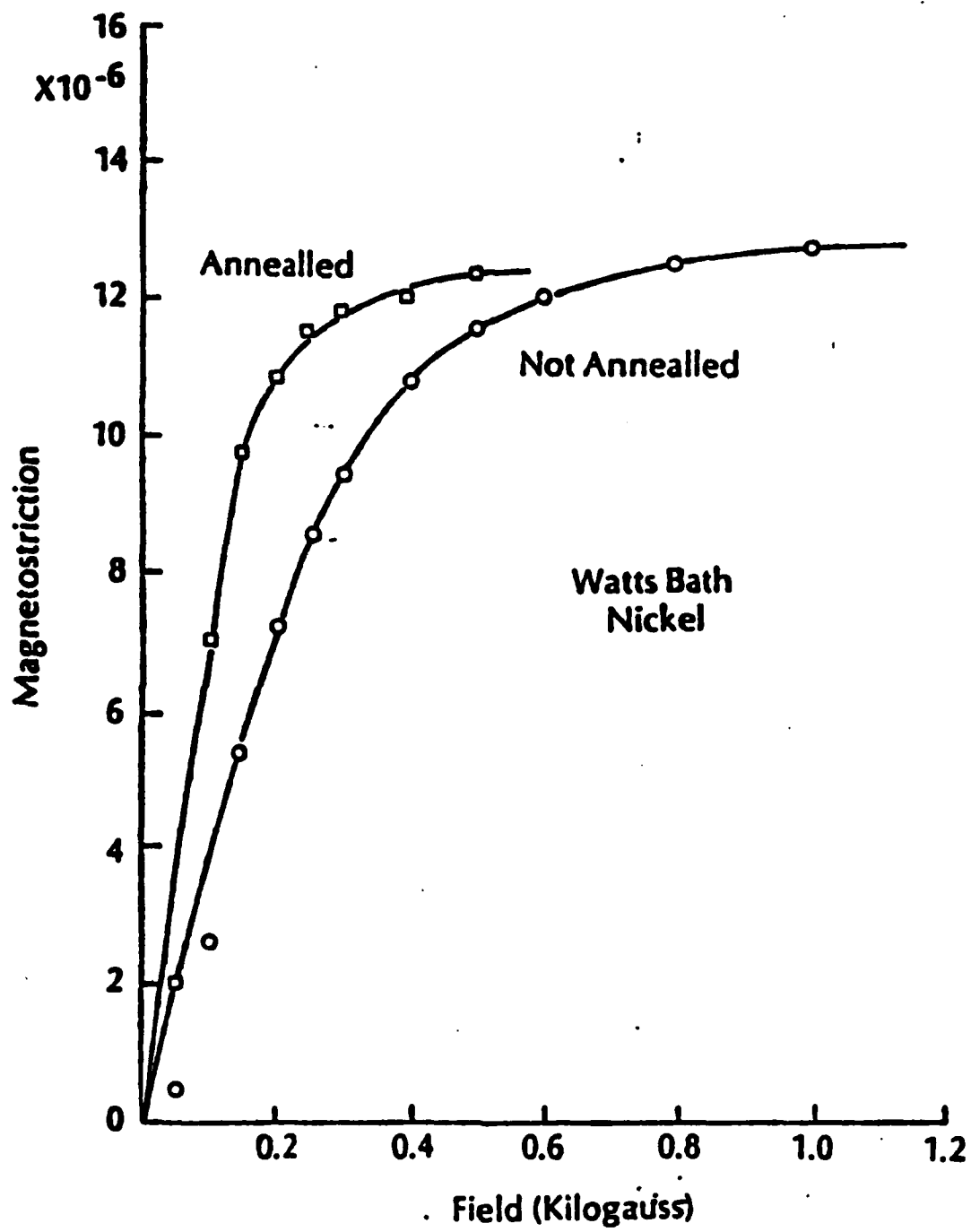


Figure 9. Magnetostriuctive strain versus magnetic field for annealed and unannealed nickel from watts bath.

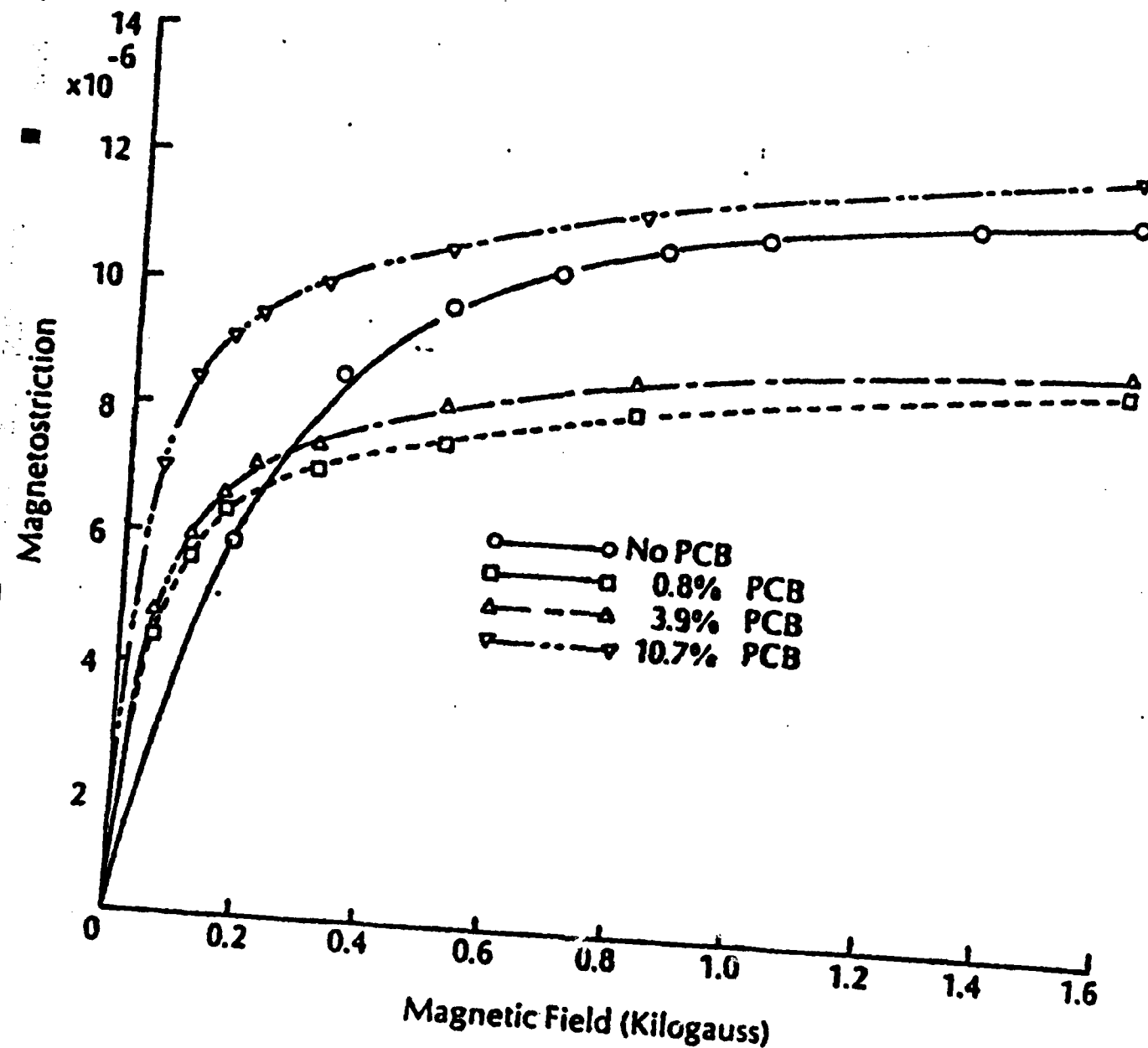


Figure 10. Magnetostriuctive strain versus field for nickel plated from sulfamate baths with varying concentrations of PCB-4 deposit modifier.

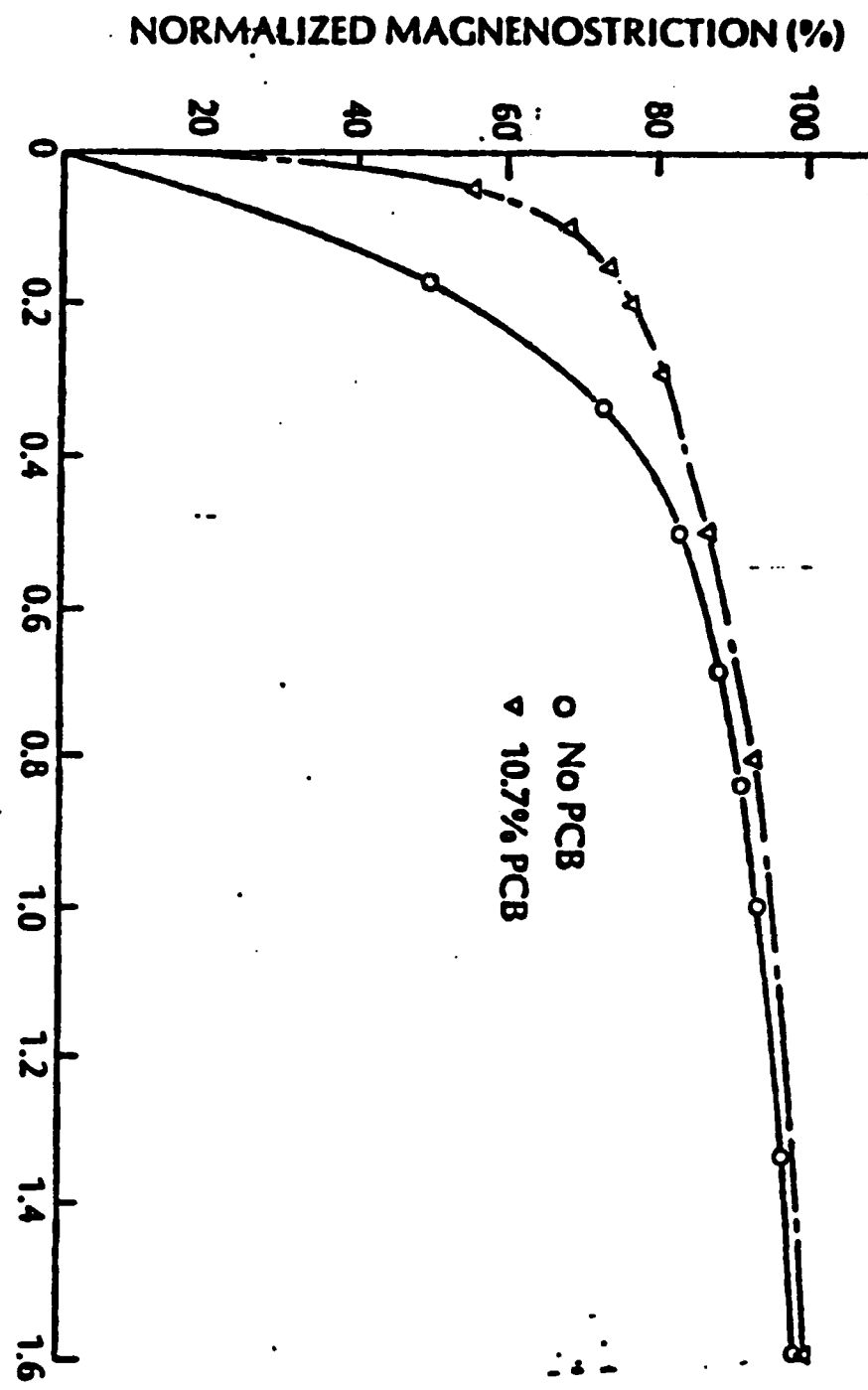
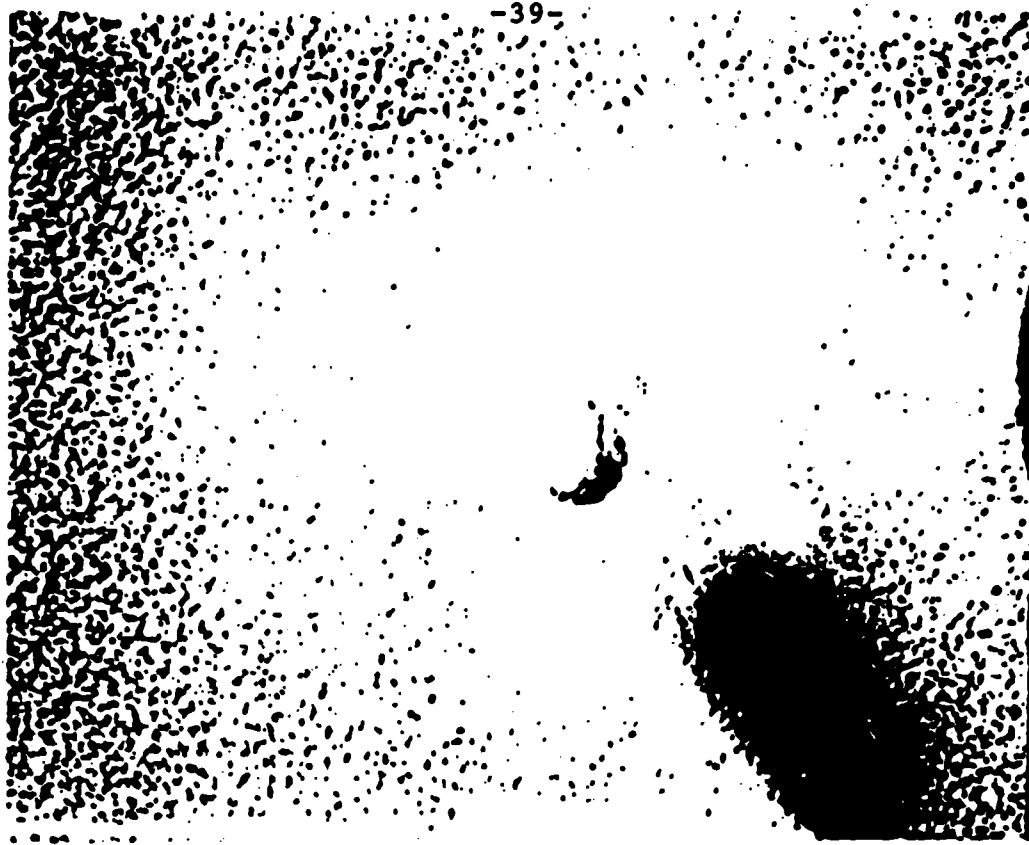


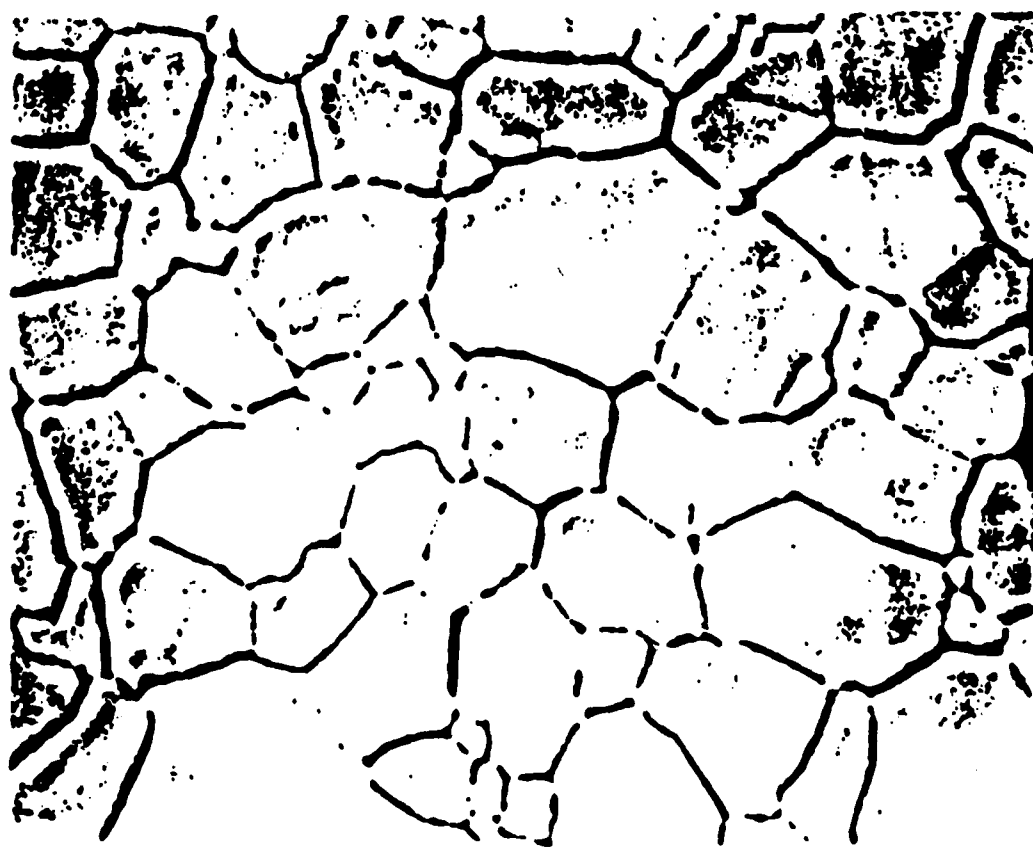
Figure 11. Normalized magnetostriuctive strain versus magnetic field for two samples from Figure 10, plated from solutions with no PCB-4 additive and with 10% PCB-4, respectively. Normalized magnetostriuctive strain is defined as magnetostriuctive strain divided by maximum strain at high field.

**C. FURTHER OBSERVATIONS**

Upon microscopic examination of the 950°C annealed samples it was noted that in each case microcracks were visible in both fibers and planar substrates. The micro cracks can be attributed to the difference in coefficient of thermal expansion between the nickel and the quartz substrate and probably occurred during cooling. A photograph of this effect is shown in Figure 12. The effect of those cracks on sensor performance is not known.



(a) Before annealing



(b) After annealing at  $950^{\circ}\text{C}$

Figure 12. Microcracks formed by annealing in electroplated Ni films.

### **VIII. FIBERS DELIVERED**

Twenty one coated fibers were delivered to NRL for test and evaluation during the contract period. All fibers were ITT single mode with chrome-copper undercoat, with the exception of the aluminum-undercoated multimode fibers provided by NRL. Ten of the fibers were for the purpose of magnetic sensitivity, where different annealing temperatures were used to try to maximize sensitivity. Eleven fibers were for the purpose of demonstrating acoustic desensitization, and different nickel thicknesses were utilized to try to reach minimum sensitivity. The fibers delivered are described in Tables V and VI.

Since the magnetic test set up at the Naval Research Laboratory tested only short  $\sim 20$  cm regions of fiber, the fibers provided for these purposes as described in Table V were relatively short, typically 1m. Nickel thickness was not critical, so it was usually in the  $14-17 \mu m$  range. The main variable was annealing, as described in Section V.

Acoustically desensitized fibers were required to be long for accurate testing, since the sensitivity per length of fiber becomes very low and it is desired to eliminate end effects in the NRL test set up. First samples were about 1m in length and subsequent samples were 3m and finally 4.5m. This is about the practical limit for the present procedure of hand stripping the fiber coatings and sputtering the undercoating layer. The key parameter for these fibers is coating thickness, which must be precisely adjusted to achieve minimum acoustic sensitivity. Initial analysis based on the elastic properties of bulk nickel, indicated minimum sensitivity would be achieved for coatings of about  $10-15 \mu m$  thickness, so several sets of fibers were prepared with thickness from 9 to  $24 \mu m$ . Subsequent testing at NRL indicated that the elastic properties of the plated Ni coatings differed from the bulk material values such that the thickness for minimum sensitivity was greater, approximately 30 to  $35 \mu m$ .

Iteration is required, based on NRL testing and analysis, to optimize the coating thickness target value. A final set of fibers, 4.5  $\mu\text{m}$  long with thicknesses of 24, 33, and 42  $\mu\text{m}$  was prepared, and is in test at NRL at this time.

TABLE V: NICKEL COATED MAGNETICALLY SENSITIVE  
FIBERS DELIVERED TO NRL

DATE	NICKEL COATING THICKNESS ( $\mu$ m)	LENGTH	QUANTITY	ANNEALING
4/8/81	14 to 15 $\mu$ m	<1 m	2	None
4/8/81	14 to 15	<1	2	950°C, H <sub>2</sub> atmosphere
6/3/81	20	0.9 to 1.2	2	None
9/24/81	16.5	1.1	1	None
9/24/81	16.5	1.1	1	400°C, H <sub>2</sub> atmosphere slow cool
9/24/81	16.5	1.1	1	600°C, H <sub>2</sub> atmosphere slow cool
9/24/81	16.1	1.2	1	950°C, H <sub>2</sub> atmosphere slow cool

TABLE VI: NICKEL COATED ACOUSTICALLY DESENSITIZED FIBERS  
DELIVERED TO NRL

DATE	NICKEL COATING THICKNESS ( $\mu$ m)	LENGTH (m)	NOTES
6/3/81	10 $\mu$ m	0.9	
6/3/81	9	0.8	
7/24/81	16	3	
7/24/81	21	3	
7/24/81	24	3	
9/24/81	8.5	3	
9/24/81	10.1	3	
9/24/81	16.5	3	
7/6/82	24	4.5	
7/6/82	33	4.5	
7/6/82	42	4.5	
			Aluminum-undercoated, multi-mode fiber supplied by NRL

## IX. CONCLUSIONS AND RECOMMENDATIONS

### A. ACOUSTICALLY DESENSITIZED FIBERS

The approach of using electrodeposited nickel coatings for the acoustic desensitization of optical fibers for sensors has been conclusively demonstrated. Results of this work using the next-to-last set of fibers (delivered to NRL on 9/24/81, as shown in Table VI) were described in a paper published in the Sept. 1982 issue of Optics Letters, jointly authored by NRL and Honeywell scientists. A copy of this paper is attached as Appendix A. Those results demonstrate acoustic sensitivity reduction by one order of magnitude below that of bare fiber.

As described in Section VIII, these fibers had not completely achieved the minimum predicted sensitivity, due to the difference in elastic properties between bulk nickel and electroplated nickel coatings. The final set of fibers, coated to a greater thickness and delivered on 7/6/82, are expected to demonstrate even more effective acoustic desensitization. At the time of this report, tests on these fibers had not been completed at NRL.

The techniques developed for undercoating and applying the nickel coating are adequate for experimental work with fibers of modest length, up to 5 or 10 m. Further development is required to make practical the coating of long lengths of 100 to 1000 m. The present technique is limited in two areas: Fiber stripping and undercoating, and the rate of nickel coating deposition.

The first of these, fiber stripping and undercoating, is the more serious limitation. Hand stripping of fiber, coated with a plastic material at the time it is drawn, is impractical in longer lengths, as is batch undercoating of a coil of fiber in a planar sputtering system. Ideally, the fiber should be coated with a conductive metal primary coating by the manufacturer at the time it is drawn. This could be by freeze coating, or some other technique. Subsequent

stripping and handling of the fibers, with degradation of fiber strength and the danger of mechanical damage would thus be eliminated, and the fiber surface would be preserved in its pristine state. Electroplating of this undercoated fiber would then be relatively straightforward, in a continuous line process. This approach was demonstrated during this contract by the nickel plating of sample fibers provided by NRL which had a freeze-coated aluminum undercoat applied by the original manufacturer. However, such metal undercoating techniques have not yet been perfected by the fiber makers and may be difficult to achieve without compromising other optical or mechanical characteristics of the fibers, such as optical loss, lifetime under stress, etc.

The second limitation is on the rate of nickel deposition: In this work, typical fiber pull speed through the plating system were about 7 cm/min. Three or four plating cells were used in series, and the length of fiber being plated in each cell is only 2 cm, for a total length of fiber being plated at any instant of only 6 to 8 cm. This can easily be scaled up by a factor of 10 or more, increasing the fiber pull speed by the same factor. This speed is still much slower than the rate at which fibers are drawn, so the nickel coating process is not compatible in speed with fiber manufacture, but the achievable speed seems high enough to be practical for coating special fibers for fiber optic sensors.

#### **B. MAGNETICALLY SENSITIZED FIBERS**

Electrodeposited nickel coatings were shown to magnetically sensitize optical fibers, as demonstrated in the coated fibers delivered to NRL by this program. Test results there show reasonable magnetic sensitivity was achieved, about equal to that using a fiber attached to a bulk nickel mandrel. However, in both cases the results fell short of what should be theoretically possible for a sensor based on magnetostriction in nickel, probably due to imperfect annealing and subsequent residual stresses. Specifically, the sensitivity reported for a bulk based sensor was  $8 \times 10^{-7}$  Gauss per meter of fiber per  $\sqrt{\text{Hz}}$

(assuming  $10^{-6}$  radius detection limit in the fiber optic interferometer), and for electroplated fiber produced under this contract sensitivity was slightly better at  $6 \times 10^{-7}$  Gauss/m- $\sqrt{\text{Hz}}$ . (By comparison, fibers using sputtered coatings of highly-magnetostrictive met glass achieved sensitivity of about  $10^{-9}$  G/m- $\sqrt{\text{Hz}}$ .)

Annealing remains a major issue with the nickel coated fibers. Good magnetic sensitivity was only obtained with those fibers annealed at high temperatures,  $950^{\circ}\text{C}$ . This temperature severely limits the choice of undercoating materials which can be employed. There is also the likelihood that cool-down from such a temperature builds stress back into the coatings due to the differential thermal expansion coefficients between the coating and the fiber, limiting the achievable magnetostrictive sensitivity to well below that theoretically possible for nickel.

To achieve higher sensitivity and perhaps a reduction in the annealing problems, while retaining the advantages of a line plating process, it is recommended that other electrodeposited magnetostrictive coating materials be investigated, specifically alloys such as Ni-Fe and Ni-Co, and possibly ternary alloys. Analysis predicts significantly higher sensitivity for fibers coated with alloys such as 40-Permalloy (40 Ni, 60 Fe) or 4.5 Co, 95.5 Ni<sup>(11)</sup>.

The issues of undercoating deposition and of scaling the electrodeposition process to higher speeds are much the same as have been discussed in the previous section. In addition, the annealing process which may be required for magnetostrictive coatings reduces the possible device of undercoating materials to those which can withstand the annealing temperature. Reduction of annealing temperature to  $600^{\circ}\text{C}$  or below would greatly ease this problem.

**X. REFERENCES**

1. G.B. Hocker, "Fiber Optic Acoustic Sensors with Composite Structure: An Analysis, "Applied Optics 18, 3679 (11/1/79)
2. S. Timoshenko and J.N. Goodier, Theory of Elasticity (McGraw-Hill, New York, New York, 1951).
3. A. Yariv and H. Winsor, Optics Letters 5, 87 (1980).
4. A. Dandridge, et al, Electronics Letters 16, 408 (1980).
5. R. Arridge and D. Heywood, Brit. J. Appl. Phys., 18, 447 (1967).
6. D. Pinnow, J. Wysocki, and G. Robertson, Trans.of the IECE of Japan, E61, No. 3, 171 (1978).
7. O. Lutes, J. Holmen, and R. Ulmer, IEEE Trans. Magn., MAG-6, 785 (1970).
8. J. Holmen and R. Ulmer, Plating Magazine, (1028 (1973).
9. Electroplating Engineering Handbook, A. Kenneth Graham (ed.), Van Nostrand Reinhold Company, New York, 1971, p. 198.
10. George Sigel, Tri-Service Workshop on Fiber Optic Sensors and Guided Wave Technology, Ft. Eustis, VA, 5-8 October 1982.
11. J. Jarzynski, et al, Applied Optics 19, 3746 (15 November 1980).

# Acoustic desensitization of single-mode fibers utilizing nickel coatings

N. Lagakos, I. J. Bush,\* J. H. Cole, and J. A. Bucaro

Naval Research Laboratory, Washington, D.C. 20375

J. D. Skogen and G. B. Hocker

Honeywell Corporation Materials Science Center, Bloomington, Minnesota 55420

Received May 10, 1982

The pressure sensitivity of the phase of light propagating in a single-mode fiber coated with a thin nickel jacket is determined both analytically and experimentally. The measured acoustic response of the fiber is found to be 1 order of magnitude lower than that of the bare fiber, in agreement with analytical predictions. The technique thus appears to be a promising way for desensitizing optical-fiber leads for use with fiber-optic sensors.

Reducing the effect of pressure on the phase of light propagating in optical fibers is important for applications involving fiber-optic interferometric sensors. In particular, in acoustic sensors of this type,<sup>1,2</sup> optimum performance is achieved when the acoustic (pressure) sensitivity is localized in the sensing fiber while the lead and reference fibers are pressure insensitive. In other devices, such as interferometric-magnetic,<sup>3,4</sup> rotation-rate,<sup>5</sup> and temperature-sensor,<sup>6</sup> acoustic sensitivity results in increased noise. It has been proposed that desensitization of optical fibers can be achieved by coating the glass-fiber waveguide with high-bulk modulus materials, such as glass<sup>7</sup> and metals.<sup>8</sup> Lagakos *et al.*<sup>9</sup> demonstrated partial desensitization utilizing thin aluminum jackets. Here we report significantly improved desensitization utilizing nickel-coated fibers.

The pressure sensitivity of the optical phase in a fiber is identified as  $\Delta\phi/\phi\Delta P$ , where  $\Delta\phi$  is the shift in the phase  $\phi$  that is due to a pressure change  $\Delta P$ . If a given pressure change  $\Delta P$  results in a fiber-core axial strain  $\epsilon_z$  and radial strain  $\epsilon_r$ , it can be shown<sup>10</sup> that

$$\Delta\phi/\phi = \epsilon_z - (n^2/2)[(P_{11} + P_{12})\epsilon_r + P_{12}\epsilon_z]. \quad (1)$$

Here  $P_{11}$  and  $P_{12}$  are the elasto-optic coefficients of the core and  $n$  is the refractive index of the core. As can be seen, the pressure sensitivity is due to the effect of the fiber-length change [first term in Eq. (1)] and to the effect of the refractive-index modulation of the core, which is related to the photoelastic effect [second and third terms in Eq. (1)]. These effects are generally of opposite polarity,<sup>7</sup> with the largest contribution coming from the axial-strain term. Accordingly, it has been proposed that substantially reduced sensitivity can be achieved if the fiber is coated with high-bulk modulus materials, which reduce the relative contribution from  $\epsilon_z$ . In fact, zero sensitivity is predicted for specific values of coating thickness that exactly balance the two effects.

Figure 1 shows the calculated sensitivity  $\Delta\phi/\phi\Delta P$  of

two fibers, an aluminum- and nickel-coated fiber, as a function of the thickness of the metal jacket. The glass fiber is a typical commercially available (ITT) single-mode fiber nominally composed of a fused-silica core with traces of  $GeO_2$ , a cladding of 5%  $B_2O_3$  + 95%  $SiO_2$ , and a fused-silica substrate in a W-shaped index profile. Table 1 lists all the parameters used to calculate the sensitivity  $\Delta\phi/\phi\Delta P$  of the fiber. As can be seen from Fig. 1, as the thickness of the metal jacket increases, the pressure sensitivity decreases rapidly; it crosses zero and then changes sign. The critical coating thickness for zero sensitivity is small for nickel ( $\sim 10.5 \mu m$ ) and relatively high for aluminum ( $\sim 95 \mu m$ ). Typical commercially available aluminum-coated fibers have metal jackets with thicknesses much smaller than  $95 \mu m$ , which results in only a partial pressure desensitization.<sup>9</sup> Because it is predicted that only a relatively thin jacket

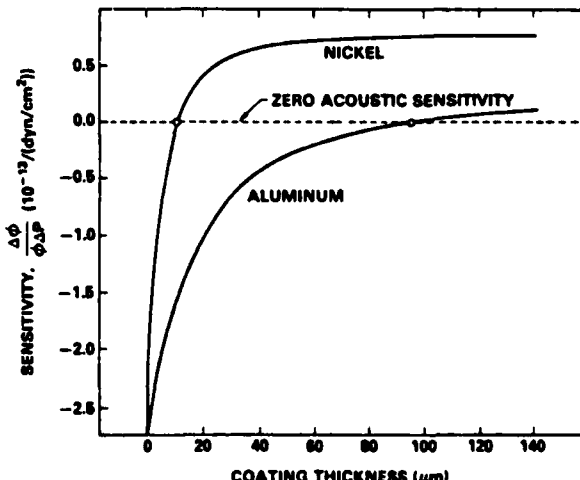


Fig. 1. Calculated pressure sensitivity  $\Delta\phi/\phi\Delta P$  versus coating thickness of the single-mode ITT bare fiber of Table 1 coated with nickel or aluminum.

Table 1. Nickel-Coated Single-Mode Fiber\*

	Core	Cladding	Substrate	First Coat-ing	Second Coat-ing
Composition	SiO <sub>2</sub> + traces of GeO <sub>2</sub> (0.1%)	95% SiO <sub>2</sub> + 5% B <sub>2</sub> O <sub>3</sub>	SiO <sub>2</sub>	Copper	Nickel
Diameter (μm)	4.0	30	86	86.8	119.8
Young's modulus (10 <sup>10</sup> dyn/cm <sup>2</sup> )	72	60	72.45	121	214
Poisson's ratio	0.17	0.18	0.17	0.37	0.336
$P_{11}$	0.126	-	-	-	-
$P_{12}$	0.27	-	-	-	-
$n$	1.459	-	-	-	-

\*  $\Delta\phi/\phi\Delta P = +0.42 \times 10^{-13}/(\text{dyn}/\text{cm}^2)$ .

of nickel is required for zero sensitivity, we coated single-mode fibers with nickel in order to study their acoustic response.

The nickel coating was applied to the fiber by electrodeposition. Conductive underlayers were first applied to the fiber by stripping it off its polymer jacket and then rf sputtering 400 Å of chromium followed by 4000 Å of copper. A nickel sulfamate plating bath was used to apply the nickel.<sup>11</sup> The plating was performed by continuously pulling the fiber through a series of four plating cells while controlling the velocity of the fiber and the plating current. Either a mercury contact or a rolling metal cylinder was used to transfer current to the fiber. Nickel anodes were used in the plating cells. Typical current density in each cell was about 450 mA/cm<sup>2</sup>, and pulling velocity was about 4 cm/min. These conditions were controlled to yield the desired coating thickness near 15 μm.

An acoustic coupler was used to produce the acoustically induced optical phase modulation in the optical fiber while maintaining hydrostatic pressure and temperature. It contained two calibrated transducers (2.54-cm diameter, air-filled piezoelectric spheres) and a port for mounting the fiber. The maximum frequency for a uniform acoustic field inside this particular coupler was 1400 Hz with DB-grade castor oil as a fill fluid.

Figure 2 illustrates the system used to measure the optical phase modulation induced in the nickel-coated fiber by the acoustic field produced within the coupler. This system is a slight modification of one reported previously.<sup>12</sup> Light from a single-frequency He-Ne laser was coupled into an electro-optic modulator (a Bragg diffractor), which produced two spatially distinct optical beams of different frequency, each of which constituted an arm of the interferometer. Recombination of the beams produced a carrier frequency  $\omega_m$  with the acoustic information (and any other phase-producing disturbances) as side bands. The carrier signal was first processed with an automatic gain control (AGC) to maintain proper amplitude. The phase was then detected and synchronously tracked by feedback to a linear phase modulator in the reference leg. The phase modulator consisted of a length of fiber wrapped tightly around a thin-walled piezoelectric cylinder (PZT-4),<sup>13</sup> which had a flat frequency response to 40 kHz. The complete details of this system have been described elsewhere.<sup>14</sup>

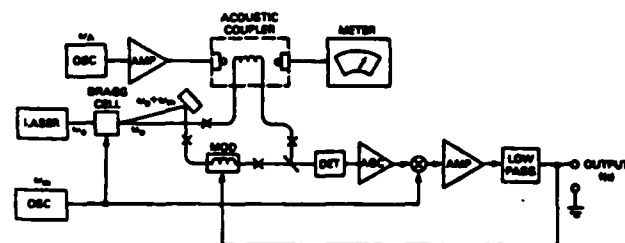


Fig. 2. Experimental setup for measuring the acoustic sensitivity of fibers.

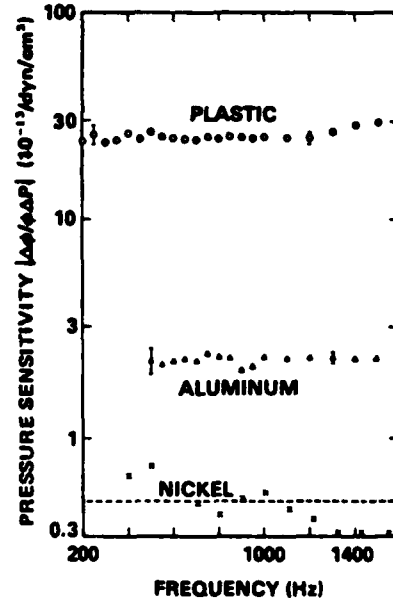


Fig. 3. Frequency response of the pressure sensitivity (absolute value) of optical fibers. Crosses, experimental data obtained from measurements on the fiber whose composition is given in Table 1. Dashed line, calculated sensitivity  $\Delta\phi/\phi\Delta P$  of the nickel-coated fiber of Table 1. Circles and triangles, experimental data obtained from measurements on a typical plastic (Hytrel)-coated ITT fiber and an aluminum-coated fiber,<sup>9</sup> respectively.

In Fig. 3 the crosses show the experimentally obtained frequency response of the sensitivity of the nickel-coated fiber. As can be seen, the sensitivity is about 1 order of magnitude lower than that for a bare fiber [ $3 \times 10^{-13}/(\text{dyn}/\text{cm}^2)$ ] and is significantly lower than that which has been achieved so far by utilizing aluminum

jackets (also shown in Fig. 3). For comparison, we also show the sensitivity of a fiber coated with a typical plastic jacket (Hytrel). The measured sensitivity of the nickel fiber was found to be in good agreement with that predicted analytically (dashed line in Fig. 3). However, since we measured only the absolute value of phase shift, we cannot claim unequivocal agreement with theory. This is a consequence of the fact that in the vicinity of zero sensitivity (see Fig. 1) the acoustically induced phase shift can be either positive or negative, depending on the exact values of coating moduli and thickness.

By utilizing a nickel jacket we have demonstrated a considerable reduction in the acoustic sensitivity of optical fibers. The technique thus appears to be a promising way (1) to localize sensitivity in interferometric fiber-optic acoustic sensors and (2) to minimize acoustic noise in thermal, magnetic, and other non-acoustic sensors.

\* Naval Research Laboratory, Underwater Sound Reference Detachment, Orlando, Florida 32856.

#### References

1. J. A. Bucaro, H. D. Dardy, and E. F. Carome, *Appl. Opt.* **16**, 1761 (1977).
2. J. H. Cole, R. L. Johnson, and R. G. Bhuta, *J. Acoust. Soc. Am.* **62**, 1136 (1977).
3. H. Aulich, N. Douklas, H. Harms, and A. Papp, in *Digest of Topical Meeting on Optical Fiber Communication* (Optical Society of America, Washington, D.C., 1979).
4. A. Dandridge, A. B. Tveten, G. H. Sigel, E. J. West, and T. G. Giallorenzi, *Electron. Lett.* **10**, 408 (1980).
5. G. Schiffner, W. Leeb, H. Krammer, and J. Wittmann, *Appl. Opt.* **18**, 2096 (1979).
6. G. B. Hocker, *Appl. Opt.* **18**, 1445 (1979).
7. N. Lagakos and J. A. Bucaro, *Appl. Opt.* **20**, 2716 (1981).
8. G. B. Hocker, presented at FOSS Workshop, Naval Research Laboratory, Washington, D.C., December 12-14, 1979.
9. N. Lagakos, T. R. Hickman, J. H. Cole, and J. A. Bucaro, *Opt. Lett.* **6**, 443 (1981).
10. B. Budiansky, D. C. Drucker, G. S. Kino, and J. R. Rice, *Appl. Opt.* **18**, 4085 (1979).
11. Harstan Technical Bulletin: *Nickel Sulfamate* (Harstan Chemical Corp., Brooklyn, N.Y.).
12. I. J. Bush, in *Digest of Conference on Lasers and Electro-Optics* (Optical Society of America, Washington, D.C., 1981).
13. D. A. Jackson, A. Dandridge, and S. K. Sheem, *Opt. Lett.* **5**, 139 (1980); D. A. Jackson, R. Priest, A. Dandridge, and A. B. Tveten, *Appl. Opt.* **19**, 2926 (1980).
14. I. J. Bush, Master's Thesis (University of Central Florida, Ocala, Fla., 1981).

